Partial wave analysis of $J/\psi \to \gamma\eta\eta'$

M. Ablikim,[1] M. N. Achasov,[10,b] P. Adlarson,[68] S. Ahmed,[14] M. Albrecht,[4] R. Aliberti,[28] A. Amoroso,[67a,67c] M. R. An,[32] Q. An,[64,50] X. H. Bai,[58] Y. Bai,[49] O. Bakina,[29] R. Baldini Ferroli,[23a] I. Balossino,[24a] Y. Ban,[39,g] V. Batozskaya,[1,37] D. Becker,[28] K. Begzsuren,[26] N. Berger,[28] M. Bertani,[23a] D. Bettoni,[24a] F. Bianchi,[67a,67c] J. Bloms,[61] A. Bortone,[67a,67c] I. Boyko,[29] R. A. Briere,[5] H. Cai,[69] X. Cai,[1,50] A. Calcaterra,[23a] G. F. Cao,[1,55] N. Cao,[1,55] S. A. Cetin,[54a] J. F. Chang,[1,50] W. L. Chang,[1,55] G. Chelkov,[29,a] C. Chen,[36] G. Chen,[1] H. S. Chen,[1,55] M. L. Chen,[1,50] S. J. Chen,[35] T. Chen,[1] X. R. Chen,[25] X. T. Chen,[1] Y. B. Chen,[1,50] Z. J. Chen,[20,h] W. S. Cheng,[67c] G. Cibinetto,[24a] F. Cossio,[67c] J. J. Cui,[42] X. F. Cui,[36] H. L. Dai,[1,50] J. P. Dai,[71] X. C. Dai,[1,55] A. Dbeyssi,[14] R. E. de Boer,[4] D. Dedovich,[29] Z. Y. Deng,[1] A. Denig,[28] I. Denysenko,[29] M. Destefanis,[67a,67c] F. De Mori,[67a,67c] Y. Ding,[33] C. Dong,[36] J. Dong,[1,50] L. Y. Dong,[1,55] M. Y. Dong,[1,50,55] X. Dong,[69] S. X. Du,[73] P. Egorov,[29,a] Y. L. Fan,[69] J. Fang,[1,50] S. S. Fang,[1,55] Y. Fang,[1] R. Farinelli,[24a] L. Fava,[67b,67c] F. Feldbauer,[4] G. Felici,[23a] C. Q. Feng,[64,50] J. H. Feng,[51] M. Fritsch,[4] C. D. Fu,[1] Y. Gao,[39,g] Y. Gao,[64,50] I. Garzia,[24a,24b] P. T. Ge,[69] C. Geng,[51] E. M. Gersabeck,[59] A. Gilman,[62] K. Goetzen,[11] L. Gong,[33] W. X. Gong,[1,50] W. Gradl,[28] M. Greco,[67a,67c] M. H. Gu,[1,50] Y. T. Gu,[74] C. Y. Guan,[1,55] A. Q. Guo,[25] A. Q. Guo,[22] L. B. Guo,[34] R. P. Guo,[41] Y. P. Guo,[9,f] A. Guskov,[29,a] T. T. Han,[42] W. Y. Han,[32] X. Q. Hao,[15] F. A. Harris,[57] K. K. He,[47] K. L. He,[1,55] F. H. Heinsius,[4] C. H. Heinz,[28] Y. K. Heng,[1,50,55] C. Herold,[52] M. Himmelreich,[11,d] T. Holtmann,[4] G. Y. Hou,[1,55] Y. R. Hou,[55] Z. L. Hou,[1] H. M. Hu,[1,55] J. F. Hu,[48,i] T. Hu,[1,50,55] Y. Hu,[1] G. S. Huang,[64,50] L. Q. Huang,[65] X. T. Huang,[42] Y. P. Huang,[1] Z. Huang,[39,g] T. Hussain,[66] N. Hüsken,[22,28] W. Ikegami Andersson,[68] W. Imoehl,[22] M. Irshad,[64,50] S. Jaeger,[4] S. Janchiv,[26] Q. Ji,[1] Q. P. Ji,[15] X. B. Ji,[1,55] X. L. Ji,[1,50] Y. Y. Ji,[42] H. B. Jiang,[42] S. S. Jiang,[32] X. S. Jiang,[1,50,55] J. B. Jiao,[42] Z. Jiao,[18] S. Jin,[35] Y. Jin,[58] M. Q. Jing,[1,55] T. Johansson,[68] N. Kalantar-Nayestanaki,[56] X. S. Kang,[33] R. Kappert,[56] M. Kavatsyuk,[56] B. C. Ke,[73] I. K. Keshk,[4] A. Khoukaz,[61] P. Kiese,[28] R. Kiuchi,[1] R. Kliemt,[11] L. Koch,[30] O. B. Kolcu,[54a] B. Kopf,[4] M. Kuemmel,[4] M. Kuessner,[4] A. Kupsc,[37,68] M. G. Kurth,[1,55] W. Kühn,[30] J. J. Lane,[59] J. S. Lange,[30] P. Larin,[14] A. Lavania,[21] L. Lavezzi,[67a,67c] Z. H. Lei,[64,50] H. Leithoff,[28] M. Lellmann,[28] T. Lenz,[28] C. Li,[40] C. Li,[36] C. H. Li,[32] Cheng Li,[64,50] D. M. Li,[73] F. Li,[1,50] G. Li,[1] H. Li,[64,50] H. Li,[44] H. B. Li,[1,55] H. J. Li,[15] H. N. Li,[48,i] J. L. Li,[42] J. Q. Li,[4] J. S. Li,[51] Ke Li,[1] L. J. Li,[1] L. K. Li,[1] Lei Li,[3] M. H. Li,[36] P. R. Li,[31,j,k] S. Y. Li,[53] T. Li,[42] W. D. Li,[1,55] W. G. Li,[1] X. H. Li,[64,50] X. L. Li,[42] Xiaoyu Li,[1,55] Z. Y. Li,[51] H. Liang,[64,50] H. Liang,[27] H. Liang,[1,55] Y. F. Liang,[46] Y. T. Liang,[25] G. R. Liao,[12] L. Z. Liao,[1,55] J. Libby,[21] A. Limphirat,[52] C. X. Lin,[51] D. X. Lin,[25] T. Lin,[1] B. J. Liu,[1] C. X. Liu,[1] D. Liu,[14,64] F. H. Liu,[45] Fang Liu,[1] Feng Liu,[6] G. M. Liu,[48,i] H. B. Liu,[74] H. M. Liu,[1,55] Huanhuan Liu,[1] Huihui Liu,[16] J. B. Liu,[64,50] J. L. Liu,[65] J. Y. Liu,[1,55] K. Liu,[1] K. Y. Liu,[33] Ke Liu,[17] L. Liu,[64,50] M. H. Liu,[9,f] P. L. Liu,[1] Q. Liu,[55] S. B. Liu,[64,50] T. Liu,[1,55] T. Liu,[9,f] W. M. Liu,[64,50] X. Liu,[31,j,k] Y. Liu,[31,j,k] Y. B. Liu,[36] Z. A. Liu,[1,50,55] Z. Q. Liu,[42] X. C. Lou,[1,50,55] F. X. Lu,[51] H. J. Lu,[18] J. D. Lu,[1,55] J. G. Lu,[1,50] X. L. Lu,[1] Y. Lu,[1] Y. P. Lu,[1,50] Z. H. Lu,[1] C. L. Luo,[34] M. X. Luo,[72] T. Luo,[9,f] X. L. Luo,[1,50] X. R. Lyu,[55] Y. F. Lyu,[36] F. C. Ma,[33] H. L. Ma,[1] L. L. Ma,[42] M. M. Ma,[1,55] Q. M. Ma,[1] R. Q. Ma,[1,55] R. T. Ma,[55] X. X. Ma,[1,55] X. Y. Ma,[1,50] Y. Ma,[39,g] F. E. Maas,[14] M. Maggiora,[67a,67c] S. Maldaner,[4] S. Malde,[62] Q. A. Malik,[66] A. Mangoni,[23b] Y. J. Mao,[39,g] Z. P. Mao,[1] S. Marcello,[67a,67c] Z. X. Meng,[58] J. G. Messchendorp,[56] G. Mezzadri,[24a] H. Miao,[1] T. J. Min,[35] R. E. Mitchell,[22] X. H. Mo,[1,50,55] N. Yu. Muchnoi,[10,b] H. Muramatsu,[60] S. Nakhoul,[11,d] Y. Nefedov,[29] F. Nerling,[11,d] I. B. Nikolaev,[10,b] Z. Ning,[1,50] S. Nisar,[8,l] S. L. Olsen,[55] Q. Ouyang,[1,50,55] S. Pacetti,[23b,23c] X. Pan,[9,f] Y. Pan,[59] A. Pathak,[1] A. Pathak,[27] P. Patteri,[23a] M. Pelizaeus,[4] H. P. Peng,[64,50] K. Peters,[11,d] J. Pettersson,[68] J. L. Ping,[34] R. G. Ping,[1,55] S. Plura,[28] S. Pogodin,[29] R. Poling,[60] V. Prasad,[64,50] H. Qi,[64,50] H. R. Qi,[53] M. Qi,[35] T. Y. Qi,[9,f] S. Qian,[1,50] W. B. Qian,[55] Z. Qian,[51] C. F. Qiao,[55] J. J. Qin,[65] L. Q. Qin,[12] X. P. Qin,[9,f] X. S. Qin,[42] Z. H. Qin,[1,50] J. F. Qiu,[1] S. Q. Qu,[36] K. H. Rashid,[66] K. Ravindran,[21] C. F. Redmer,[28] K. J. Ren,[32] A. Rivetti,[67c] V. Rodin,[56] M. Rolo,[67c] G. Rong,[1,55] Ch. Rosner,[14] M. Rump,[61] H. S. Sang,[64] A. Sarantsev,[29,c] Y. Schelhaas,[28] C. Schnier,[4] K. Schoenning,[68] M. Scodeggio,[24a,24b] W. Shan,[19] X. Y. Shan,[64,50] J. F. Shangguan,[47] L. G. Shao,[1,55] M. Shao,[64,50] C. P. Shen,[9,f] H. F. Shen,[1,55] X. Y. Shen,[1,55] B.-A. Shi,[55] H. C. Shi,[64,50] R. S. Shi,[1,55] X. Shi,[1,50] X. D. Shi,[64,50] J. J. Song,[15] W. M. Song,[27,1] Y. X. Song,[39,g] S. Sosio,[67a,67c] S. Spataro,[67a,67c] F. Stieler,[28] K. X. Su,[69] P. P. Su,[47] Y.-J. Su,[55] G. X. Sun,[1] H. K. Sun,[1] J. F. Sun,[15] L. Sun,[69] S. S. Sun,[1,55] T. Sun,[1,55] W. Y. Sun,[27] X. Sun,[20,h] Y. J. Sun,[64,50] Y. Z. Sun,[1] Z. T. Sun,[42] Y. H. Tan,[69] Y. X. Tan,[64,50] C. J. Tang,[46] G. Y. Tang,[1] J. Tang,[51] Q. T. Tao,[20,h] J. X. Teng,[64,50] V. Thoren,[68] W. H. Tian,[44] Y. T. Tian,[25] I. Uman,[54b] B. Wang,[1] D. Y. Wang,[39,g] H. J. Wang,[31,j,k] H. P. Wang,[1,55] K. Wang,[1,50] L. L. Wang,[1] M. Wang,[42] M. Z. Wang,[39,g] Meng Wang,[1,55] S. Wang,[9,f] T. J. Wang,[36] W. Wang,[51] W. H. Wang,[69] W. P. Wang,[64,50] X. Wang,[39,g] X. F. Wang,[31,j,k] X. L. Wang,[9,f] Y. Wang,[51] Y. D. Wang,[38] Y. F. Wang,[1,50,55] Y. Q. Wang,[1] Y. Y. Wang,[31,j,k] Z. Wang,[1,50] Z. Y. Wang,[1] Ziyi Wang,[55] Zongyuan Wang,[1,55] D. H. Wei,[12] F. Weidner,[61] S. P. Wen,[1] D. J. White,[59] U. Wiedner,[4] G. Wilkinson,[62] M. Wolke,[68] L. Wollenberg,[4] J. F. Wu,[1,55] L. H. Wu,[1] L. J. Wu,[1,55] X. Wu,[9,f] X. H. Wu,[27] Z. Wu,[1,50] L. Xia,[64,50] T. Xiang,[39,g] H. Xiao,[9,f] S. Y. Xiao,[1] Z. J. Xiao,[34] X. H. Xie,[39,g] Y. G. Xie,[1,50] Y. H. Xie,[6] T. Y. Xing,[1,55] C. F. Xu,[1] C. J. Xu,[51] G. F. Xu,[1] Q. J. Xu,[13] W. Xu,[1,55] X. P. Xu,[47] Y. C. Xu,[55] F. Yan,[9,f] L. Yan,[9,f] W. B. Yan,[64,50] W. C. Yan,[73] H. J. Yang,[43,e] H. X. Yang,[1] L. Yang,[44] S. L. Yang,[55] Y. X. Yang,[1,55] Y. X. Yang,[12]

Yifan Yang,[1,55] Zhi Yang,[25] M. Ye,[1,50] M. H. Ye,[7] J. H. Yin,[1] Z. Y. You,[51] B. X. Yu,[1,50,55] C. X. Yu,[36] G. Yu,[1,55] J. S. Yu,[20,h] T. Yu,[65] C. Z. Yuan,[1,55] L. Yuan,[2] S. C. Yuan,[1] Y. Yuan,[1] Z. Y. Yuan,[51] C. X. Yue,[32] A. A. Zafar,[66] X. Zeng,[6] Y. Zeng,[20,h] A. Q. Zhang,[1] B. L. Zhang,[1] B. X. Zhang,[1] G. Y. Zhang,[15] H. Zhang,[64] H. H. Zhang,[27] H. H. Zhang,[51] H. Y. Zhang,[1,50] J. L. Zhang,[70] J. Q. Zhang,[34] J. W. Zhang,[1,50,55] J. Y. Zhang,[1] J. Z. Zhang,[1,55] Jianyu Zhang,[1,55] Jiawei Zhang,[1,55] L. M. Zhang,[53] L. Q. Zhang,[51] Lei Zhang,[35] P. Zhang,[1] Shulei Zhang,[20,h] X. D. Zhang,[38] X. M. Zhang,[1] X. Y. Zhang,[47] X. Y. Zhang,[42] Y. Zhang,[62] Y. T. Zhang,[73] Y. H. Zhang,[1,50] Yan Zhang,[64,50] Yao Zhang,[1] Z. H. Zhang,[1] Z. Y. Zhang,[36] Z. Y. Zhang,[69] G. Zhao,[1] J. Zhao,[32] J. Y. Zhao,[1,55] J. Z. Zhao,[1,50] Lei Zhao,[64,50] Ling Zhao,[1] M. G. Zhao,[36] Q. Zhao,[1] S. J. Zhao,[73] Y. B. Zhao,[1,50] Y. X. Zhao,[25] Z. G. Zhao,[64,50] A. Zhemchugov,[29,a] B. Zheng,[65] J. P. Zheng,[1,50] Y. H. Zheng,[55] B. Zhong,[34] C. Zhong,[65] L. P. Zhou,[1,55] Q. Zhou,[1,55] X. Zhou,[69] X. K. Zhou,[55] X. R. Zhou,[64,50] X. Y. Zhou,[32] A. N. Zhu,[1,55] J. Zhu,[36] K. Zhu,[1] K. J. Zhu,[1,50,55] S. H. Zhu,[63] T. J. Zhu,[70] W. J. Zhu,[36] W. J. Zhu,[9,f] Y. C. Zhu,[64,50] Z. A. Zhu,[1,55] B. S. Zou,[1] and J. H. Zou[1]

(BESIII Collaboration)

[1]*Institute of High Energy Physics, Beijing 100049, People's Republic of China*
[2]*Beihang University, Beijing 100191, People's Republic of China*
[3]*Beijing Institute of Petrochemical Technology, Beijing 102617, People's Republic of China*
[4]*Bochum Ruhr-University, D-44780 Bochum, Germany*
[5]*Carnegie Mellon University, Pittsburgh, Pennsylvania 15213, USA*
[6]*Central China Normal University, Wuhan 430079, People's Republic of China*
[7]*China Center of Advanced Science and Technology, Beijing 100190, People's Republic of China*
[8]*COMSATS University Islamabad, Lahore Campus, Defence Road,*
Off Raiwind Road, 54000 Lahore, Pakistan
[9]*Fudan University, Shanghai 200443, People's Republic of China*
[10]*G.I. Budker Institute of Nuclear Physics SB RAS (BINP), Novosibirsk 630090, Russia*
[11]*GSI Helmholtzcentre for Heavy Ion Research GmbH, D-64291 Darmstadt, Germany*
[12]*Guangxi Normal University, Guilin 541004, People's Republic of China*
[13]*Hangzhou Normal University, Hangzhou 310036, People's Republic of China*
[14]*Helmholtz Institute Mainz, Staudinger Weg 18, D-55099 Mainz, Germany*
[15]*Henan Normal University, Xinxiang 453007, People's Republic of China*
[16]*Henan University of Science and Technology, Luoyang 471003, People's Republic of China*
[17]*Henan University of Technology, Zhengzhou 450001, People's Republic of China*
[18]*Huangshan College, Huangshan 245000, People's Republic of China*
[19]*Hunan Normal University, Changsha 410081, People's Republic of China*
[20]*Hunan University, Changsha 410082, People's Republic of China*
[21]*Indian Institute of Technology Madras, Chennai 600036, India*
[22]*Indiana University, Bloomington, Indiana 47405, USA*
[23a]*INFN Laboratori Nazionali di Frascati, I-00044 Frascati, Italy*
[23b]*INFN Sezione di Perugia, I-06100 Perugia, Italy*
[23c]*University of Perugia, I-06100 Perugia, Italy*
[24a]*INFN Sezione di Ferrara, I-44122 Ferrara, Italy*
[24b]*University of Ferrara, I-44122 Ferrara, Italy*
[25]*Institute of Modern Physics, Lanzhou 730000, People's Republic of China*
[26]*Institute of Physics and Technology, Peace Ave. 54B, Ulaanbaatar 13330, Mongolia*
[27]*Jilin University, Changchun 130012, People's Republic of China*
[28]*Johannes Gutenberg University of Mainz, Johann-Joachim-Becher-Weg 45, D-55099 Mainz, Germany*
[29]*Joint Institute for Nuclear Research, 141980 Dubna, Moscow region, Russia*
[30]*Justus-Liebig-Universitaet Giessen, II. Physikalisches Institut,*
Heinrich-Buff-Ring 16, D-35392 Giessen, Germany
[31]*Lanzhou University, Lanzhou 730000, People's Republic of China*
[32]*Liaoning Normal University, Dalian 116029, People's Republic of China*
[33]*Liaoning University, Shenyang 110036, People's Republic of China*
[34]*Nanjing Normal University, Nanjing 210023, People's Republic of China*
[35]*Nanjing University, Nanjing 210093, People's Republic of China*
[36]*Nankai University, Tianjin 300071, People's Republic of China*
[37]*National Centre for Nuclear Research, Warsaw 02-093, Poland*
[38]*North China Electric Power University, Beijing 102206, People's Republic of China*
[39]*Peking University, Beijing 100871, People's Republic of China*
[40]*Qufu Normal University, Qufu 273165, People's Republic of China*

[41] *Shandong Normal University, Jinan 250014, People's Republic of China*
[42] *Shandong University, Jinan 250100, People's Republic of China*
[43] *Shanghai Jiao Tong University, Shanghai 200240, People's Republic of China*
[44] *Shanxi Normal University, Linfen 041004, People's Republic of China*
[45] *Shanxi University, Taiyuan 030006, People's Republic of China*
[46] *Sichuan University, Chengdu 610064, People's Republic of China*
[47] *Soochow University, Suzhou 215006, People's Republic of China*
[48] *South China Normal University, Guangzhou 510006, People's Republic of China*
[49] *Southeast University, Nanjing 211100, People's Republic of China*
[50] *State Key Laboratory of Particle Detection and Electronics,*
Beijing 100049, Hefei 230026, People's Republic of China
[51] *Sun Yat-Sen University, Guangzhou 510275, People's Republic of China*
[52] *Suranaree University of Technology, University Avenue 111, Nakhon Ratchasima 30000, Thailand*
[53] *Tsinghua University, Beijing 100084, People's Republic of China*
[54a] *Turkish Accelerator Center Particle Factory Group, Istinye University, 34010, Istanbul, Turkey*
[54b] *Near East University, Nicosia, North Cyprus, Mersin 10, Turkey*
[55] *University of Chinese Academy of Sciences, Beijing 100049, People's Republic of China*
[56] *University of Groningen, NL-9747 AA Groningen, Netherlands*
[57] *University of Hawaii, Honolulu, Hawaii 96822, USA*
[58] *University of Jinan, Jinan 250022, People's Republic of China*
[59] *University of Manchester, Oxford Road, Manchester, M13 9PL, United Kingdom*
[60] *University of Minnesota, Minneapolis, Minnesota 55455, USA*
[61] *University of Muenster, Wilhelm-Klemm-Str. 9, 48149 Muenster, Germany*
[62] *University of Oxford, Keble Rd, Oxford, United Kingdom OX13RH*
[63] *University of Science and Technology Liaoning, Anshan 114051, People's Republic of China*
[64] *University of Science and Technology of China, Hefei 230026, People's Republic of China*
[65] *University of South China, Hengyang 421001, People's Republic of China*
[66] *University of the Punjab, Lahore-54590, Pakistan*
[67a] *University of Turin and INFN, University of Turin, I-10125 Turin, Italy*
[67b] *University of Eastern Piedmont, I-15121 Alessandria, Italy*
[67c] *INFN, I-10125 Turin, Italy*
[68] *Uppsala University, Box 516, SE-75120 Uppsala, Sweden*
[69] *Wuhan University, Wuhan 430072, People's Republic of China*
[70] *Xinyang Normal University, Xinyang 464000, People's Republic of China*
[71] *Yunnan University, Kunming 650500, People's Republic of China*
[72] *Zhejiang University, Hangzhou 310027, People's Republic of China*
[73] *Zhengzhou University, Zhengzhou 450001, People's Republic of China*
[74] *Guangxi University, Nanning 530004, People's Republic of China*

[a] Also at the Moscow Institute of Physics and Technology, Moscow 141700, Russia.
[b] Also at the Novosibirsk State University, Novosibirsk, 630090, Russia.
[c] Also at the NRC "Kurchatov Institute", PNPI, 188300, Gatchina, Russia.
[d] Also at Goethe University Frankfurt, 60323 Frankfurt am Main, Germany.
[e] Also at Key Laboratory for Particle Physics, Astrophysics and Cosmology, Ministry of Education; Shanghai Key Laboratory for Particle Physics and Cosmology; Institute of Nuclear and Particle Physics, Shanghai 200240, People's Republic of China.
[f] Also at Key Laboratory of Nuclear Physics and Ion-beam Application (MOE) and Institute of Modern Physics, Fudan University, Shanghai 200443, People's Republic of China.
[g] Also at State Key Laboratory of Nuclear Physics and Technology, Peking University, Beijing 100871, People's Republic of China.
[h] Also at School of Physics and Electronics, Hunan University, Changsha 410082, China.
[i] Also at Guangdong Provincial Key Laboratory of Nuclear Science, Institute of Quantum Matter, South China Normal University, Guangzhou 510006, China.
[j] Also at Frontiers Science Center for Rare Isotopes, Lanzhou University, Lanzhou 730000, People's Republic of China.
[k] Also at Lanzhou Center for Theoretical Physics, Lanzhou University, Lanzhou 730000, People's Republic of China.
[l] Also at the Department of Mathematical Sciences, IBA, Karachi, Pakistan.

Based on a sample of $(10.09 \pm 0.04) \times 10^9$ J/ψ events collected with the BESIII detector operating at the BEPCII storage ring, a partial wave analysis of the decay $J/\psi \to \gamma\eta\eta'$ is performed. An isoscalar state with exotic quantum numbers $J^{PC} = 1^{-+}$, denoted as $\eta_1(1855)$, has been observed for the first time with statistical significance larger than 19σ. Its mass and width are measured to be $(1855 \pm 9^{+6}_{-1})$ MeV/c^2 and $(188 \pm 18^{+3}_{-8})$ MeV, respectively. The first uncertainties are statistical and the second are systematic. The product branching fraction $\mathcal{B}(J/\psi \to \gamma\eta_1(1855))\mathcal{B}(\eta_1(1855) \to \eta\eta')$ is measured to be $(2.70 \pm 0.41^{+0.16}_{-0.35}) \times 10^{-6}$. In addition, an upper limit on the ratio of branching fractions $\mathcal{B}(f_0(1710) \to \eta\eta')/\mathcal{B}(f_0(1710) \to \pi\pi)$ is determined to be 1.61×10^{-3} at 90% confidence level, which lends support to the hypothesis that the $f_0(1710)$ has a large glueball component.

I. INTRODUCTION

Confinement is a unique property of quantum chromodynamics (QCD), and can be probed via the spectrum of mesons. While the quark model describes a conventional meson as a bound state of a quark and an antiquark, lattice QCD (LQCD) and QCD-motivated models predict a more rich spectrum of mesons that includes bound states with gluonic degrees of freedom, such as glueballs and hybrids. Radiative decays of the J/ψ meson provide a gluon-rich environment and are therefore regarded as one of the most promising hunting grounds for gluonic excitations [1–4].

The spectrum of glueballs, states composed of only gluons, is predicted by quenched LQCD [5–7]. The lightest glueball is expected to have scalar quantum numbers, $J^{PC} = 0^{++}$, and a mass between 1.5 and 1.7 GeV/c^2 [6,7]. LQCD calculations also predict that the branching fraction of the J/ψ radiatively decaying into a pure scalar glueball is $3.8(9) \times 10^{-3}$ [3,4,8]. The $f_0(1710)$ is a strong candidate for the lightest glueball, but this identification is complicated by possible mixing with conventional mesons. Recent partial wave analyses (PWA) of $J/\psi \to \gamma\eta\eta$ [9] and $J/\psi \to \gamma K_S K_S$ [10] by BESIII show that the product branching fractions $\mathcal{B}(J/\psi \to \gamma f_0) \times \mathcal{B}(f_0 \to \eta\eta \text{ or } K_S K_S)$ are one order of magnitude larger for the $f_0(1710)$ than for the $f_0(1500)$. Furthermore, the total measured branching fraction of $J/\psi \to \gamma f_0(1710)$, summing over all observed $f_0(1710)$ decay modes, is currently 1.7×10^{-3} [11], which is compatible with LQCD calculations for a scalar glueball [8]. Since glueball decays to the $\eta\eta'$ final state are suppressed due to gauge duality [12], the $\eta\eta'$ final state is a crucial probe for distinguishing glueballs from conventional mesons [13]. Assuming the glueball branching ratio $\mathcal{B}(G \to KK)/\mathcal{B}(G \to \pi\pi)$ is within the range of those measured for the $f_0(1710)$ in the Review of Particle Physics by Particle Data Group (PDG) [14], Ref. [12] predicts the ratio $\mathcal{B}(G \to \eta\eta')/\mathcal{B}(G \to \pi\pi)$ to be less than 0.04.

Hybrid mesons are an additional type of QCD exotic state with gluonic degrees of freedom. They were first proposed several decades ago [15–19], and have been the source of more recent LQCD [20–23] and phenomenological QCD

studies [24–27]. Models and LQCD predict that the exotic $J^{PC} = 1^{-+}$ nonet of hybrid mesons is the lightest, with a mass around 1.7–2.1 GeV/c^2 [20,23,28]. The predicted decay widths are model-dependent; most hybrids are expected to be rather broad, but some can be as narrow as 100 MeV [29]. To date, there has been experimental evidence for as many as three isovector states with exotic quantum numbers $J^{PC} = 1^{-+}$: the $\pi_1(1400)$, $\pi_1(1600)$, and $\pi_1(2015)$ [30–33]. Finding an isoscalar 1^{-+} hybrid state is critical for establishing the hybrid multiplet. Decaying to $\eta\eta'$ in a P-wave is expected for an isoscalar 1^{-+} hybrid state [34–36].

In this paper, based on a sample of $(10.09 \pm 0.04) \times 10^9$ J/ψ events collected with the BESIII detector [37], we present a partial wave analysis of $J/\psi \to \gamma\eta\eta'$ to search for 1^{-+} and investigate the decay property of $f_0(1710)$. The η is reconstructed via the decay channel $\gamma\gamma$, and the η' is reconstructed via the decay channels $\eta' \to \gamma\pi^+\pi^-$ and $\eta' \to \eta\pi^+\pi^-$. This paper is accompanied by a letter submitted to Physical Review Letters [38].

II. BESIII DETECTOR AND MONTE CARLO SIMULATION

The BESIII detector [39] records symmetric e^+e^- collisions provided by the BEPCII storage ring, which operates with a peak luminosity of 1×10^{33} cm^{-2} s^{-1} at the center-of-mass energy 3.89 GeV. BESIII has collected large data samples in the energy region between 2.0 and 4.9 GeV [40]. The cylindrical core of the BESIII detector covers 93% of the full solid angle and consists of a helium-based multilayer drift chamber (MDC), a plastic scintillator time-of-flight system (TOF), and a CsI(Tl) electromagnetic calorimeter (EMC), which are all enclosed in a superconducting solenoidal magnet providing a 1.0 T (0.9 T in 2012) magnetic field. The solenoid is supported by an octagonal flux-return yoke with resistive plate counter muon identification modules interleaved with steel. The charged-particle momentum resolution at 1 GeV/c is 0.5%, and the dE/dx resolution is 6% for electrons The EMC measures photon energies with a resolution of 2.5% (5%) at 1 GeV in the barrel (end cap) region. The time resolution in the TOF barrel region is 68 ps, while that in

the end cap region is 110 ps. The end cap TOF system was upgraded in 2015 using multigap resistive plate chamber technology, providing a time resolution of 60 ps [41–43].

Simulated data samples produced with a GEANT4-based [44] Monte Carlo (MC) package, which includes the geometric description of the BESIII detector and the detector response, are used to optimize the event selection criteria, to determine detection efficiencies, and to estimate backgrounds. Signal MC samples for the process $J/\psi \to \gamma\eta\eta'$ with the subsequent decays $\eta \to \gamma\gamma$ and $\eta' \to \eta\pi^+\pi^-$ are generated uniformly in phase space. The decay $\eta' \to \gamma\pi^+\pi^-$ is simulated by taking into account both $\rho - \omega$ interference and the box anomaly [45].

An inclusive MC sample with $10.01 \times 10^9 J/\psi$ decays is used to study backgrounds. The known decay modes are modeled with EVTGEN [46] by incorporating branching fractions taken from the Particle Data Group [14], and the remaining unknown decays are generated using the LUNDCHARM [47] generator. The simulation includes the beam energy spread and initial state radiation (ISR) in the e^+e^- annihilations modeled with the generator KKMC [48]. Final state radiation (FSR) from charged particles is incorporated with the PHOTOS package [49].

III. EVENT SELECTION

Charged tracks are reconstructed from hits in the MDC and are required to have $|\cos\theta| < 0.93$, where θ is the polar angle defined with respect to the symmetry axis of the MDC in the laboratory frame. Tracks must approach within 10 cm of the interaction point in the beam direction and 1 cm in the plane perpendicular to the beam where the distances are defined in the laboratory frame. Each track is assumed to be a pion, and no particle identification is applied.

Photon candidates are required to have energy deposition above 25 MeV in the barrel region ($|\cos\theta| < 0.80$) or 50 MeV in the end caps ($0.86 < |\cos\theta| < 0.92$). To exclude spurious photons caused by hadronic interactions and final state radiation, photon candidates must be at least 10° away from any charged tracks when extrapolated to the EMC. To suppress spurious photons due to electronic noise or energy deposits unrelated to the event, candidate showers are required to occur within 700 ns of the event start time.

For the $J/\psi \to \gamma\eta\eta'$, $\eta' \to \gamma\pi^+\pi^-$ channel, events are reconstructed with two oppositely charged tracks and at least four candidate photons. A five-constraint (5C) kinematic fit under the hypothesis $J/\psi \to \gamma\gamma\eta\pi^+\pi^-$ is performed by constraining energy-momentum conservation and the mass of one pair of photons to the nominal mass of the η (m_η) from the PDG [14]. If there is more than one combination, the combination with the minimum χ^2_{5C} is retained. The resulting χ^2_{5C} is required to be less than 15. To suppress backgrounds from processes with three or five photons in the final state, four-constraint (4C) kinematic

fits are performed by constraining energy-momentum conservation under the hypotheses $J/\psi \to 3\gamma\pi^+\pi^-$, $J/\psi \to 4\gamma\pi^+\pi^-$, and $J/\psi \to 5\gamma\pi^+\pi^-$. The $\chi^2_{4C}(4\gamma\pi^+\pi^-)$ is required to be less than all possible $\chi^2_{4C}(3\gamma\pi^+\pi^-)$ and $\chi^2_{4C}(5\gamma\pi^+\pi^-)$. To reconstruct the η' candidate, the $\gamma\pi^+\pi^-$ combination with the minimum $|M(\gamma\pi^+\pi^-) - m_{\eta'}|$ is chosen, where $m_{\eta'}$ is the nominal mass of the η' taken from the PDG [14]. The invariant mass distribution of $\gamma\pi^+\pi^-$ is shown in Fig. 1(a). Events with $|M(\gamma\pi^+\pi^-) - m_{\eta'}| < 0.015$ GeV/c^2 are selected for further analysis. The $\pi^+\pi^-$ invariant mass is required to be near the ρ^0 mass region, $0.6 < M(\pi^+\pi^-) < 0.8$ GeV/c^2. To suppress backgrounds containing π^0 and backgrounds due to misreconstructed η, events with $|M(\gamma\gamma) - m_{\pi^0}| < 0.04$ or $|M(\gamma\gamma) - m_\eta| < 0.02$ GeV/c^2 are rejected, where $M(\gamma\gamma)$ are the invariant masses of all photon pairs except the photon pair assigned to the η and m_{π^0} is the nominal mass of the π^0 [14]. There is a clear ϕ signal in the $\gamma\eta$ invariant mass distribution corresponding to $J/\psi \to \phi\eta'$, $\phi \to \gamma\eta$. Since detector resolution is difficult to model in partial wave analyses, and since the process $J/\psi \to \phi\eta'$ is not our primary interest, we exclude it by rejecting events with $|M(\gamma\eta) - m_\phi| < 0.04$ GeV/c^2. According to the study of inclusive MC, in order to further reduce the background from $J/\psi \to 3\gamma\pi^+\pi^-$ with spurious photons, only events with $M(\eta\eta') < 2.95$ GeV/c^2 are chosen for further analysis.

For the $J/\psi \to \gamma\eta\eta'$, $\eta' \to \eta\pi^+\pi^-$ channel, events are reconstructed with two oppositely charged tracks and at least five candidate photons. A six-constraint (6C) kinematic fit under the hypothesis $J/\psi \to \gamma\eta\eta\pi^+\pi^-$ is performed by constraining energy-momentum conservation and the masses of two pairs of photons to m_η. If there is more than one combination, the combination with the minimum χ^2_{6C} is retained. The resulting χ^2_{6C} is required to be less than 45. To suppress backgrounds with four or six photons in the final state, 4C kinematic fits are performed by constraining energy-momentum conservation under the hypotheses $J/\psi \to 4\gamma\pi^+\pi^-$, $J/\psi \to 5\gamma\pi^+\pi^-$, and $J/\psi \to 6\gamma\pi^+\pi^-$. The $\chi^2_{4C}(5\gamma\pi^+\pi^-)$ is required to be less than all possible $\chi^2_{4C}(4\gamma\pi^+\pi^-)$ and $\chi^2_{4C}(6\gamma\pi^+\pi^-)$. The $\eta\pi^+\pi^-$ combination with the minimum $|M(\eta\pi^+\pi^-) - m_{\eta'}|$ is used to reconstruct the η' candidate. The invariant mass distribution of $\eta\pi^+\pi^-$ is shown in Fig. 1(b). Events with $|M(\eta\pi^+\pi^-) - m_{\eta'}| < 0.01$ GeV/c^2 are selected for further analysis. Backgrounds containing a π^0 and backgrounds due to misreconstructed η are suppressed by rejecting events with $|M(\gamma\gamma) - m_{\pi^0}| < 0.03$ or $|M(\gamma\gamma) - m_\eta| < 0.02$ GeV/c^2, respectively. To exclude $J/\psi \to \phi\eta'$, $\phi \to \gamma\eta$, events with $|M(\gamma\eta) - m_\phi| < 0.04$ GeV/c^2 are rejected.

The invariant mass distributions of $\eta\eta'$ and the Dalitz plot for the selected $\gamma\eta\eta'$ candidate events from the two decay channels are shown in Figs. 1(c)–1(f), respectively.
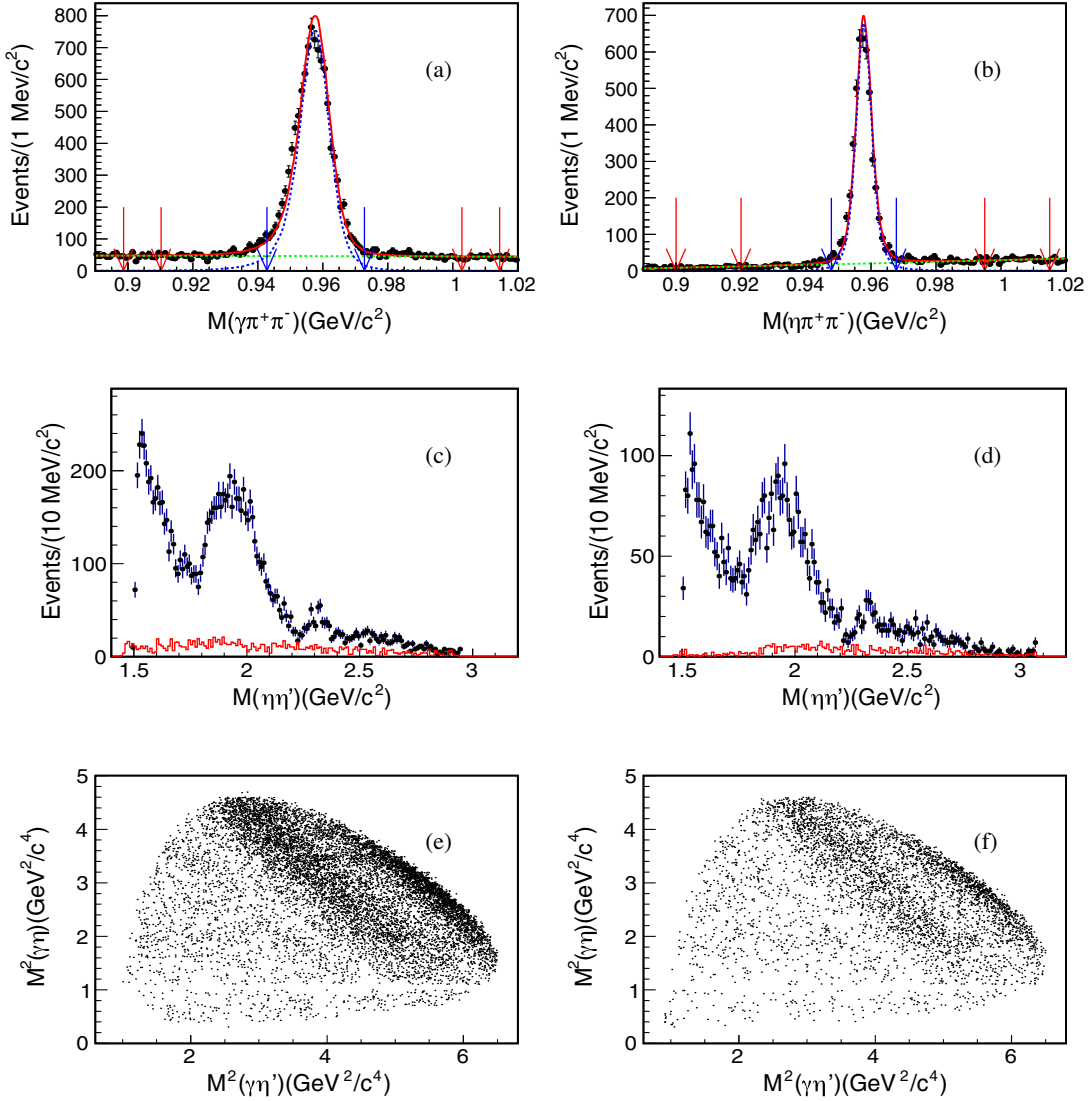
FIG. 1.   Invariant mass distributions for (a,c,e) $J/\psi \to \gamma\eta\eta'$, $\eta' \to \gamma\pi^+\pi^-$ and (b,d,f) $J/\psi \to \gamma\eta\eta'$, $\eta' \to \eta\pi^+\pi^-$. (a,b) Invariant mass distributions for η' candidates. The events between the blue arrows are the selected signal events, and events between the red arrows on the same side are selected sideband events. The black points with error bars are data, the red solid line is the fit result, the blue dashed line is the η' signal shape from signal MC, and the green dashed line is the 2nd degree polynomial function for the background. (c,d) Invariant mass distributions of the $\eta\eta'$ for the selected $\gamma\eta\eta'$ candidates. The points with error bars are data and the red line shows the background events estimated from the η' sideband. (e,f) The corresponding Dalitz plots for the selected $\gamma\eta\eta'$ candidates.

Clear structures in the $\eta\eta'$ invariant mass spectrum are observed.

Potential backgrounds are studied using the inclusive MC sample of 10.01×10^9 J/ψ decays (as described in Sec. II). No significant peaking background is observed in the invariant mass distribution of the η'. Backgrounds are estimated by the η' sidebands in the data. The sideband regions of $\eta' \to \eta\pi^+\pi^-$ and $\eta' \to \gamma\pi^+\pi^-$ are defined as $M(\eta\pi^+\pi^-) \in [0.900, 0.920] \cup [0.995, 1.015]$ GeV/c^2 and $M(\gamma\pi^+\pi^-) \in [0.903, 0.915] \cup [1.000, 1.012]$ GeV/c^2, respectively. The normalization factors for events in the two sideband regions are obtained by a fit to data of the invariant mass spectrum of $M(\eta\pi^+\pi^-)$ and $M(\gamma\pi^+\pi^-)$.

The η' signal shapes are determined from the shapes of signal MC samples described with RooHistPdf [50], and the backgrounds are described by 2nd degree polynomial functions. The definition of the sidebands and the fit results are shown in Figs. 1(a) and 1(b). The background levels for $J/\psi \to \gamma\eta\eta'$, $\eta' \to \eta\pi^+\pi^-$ and $J/\psi \to \gamma\eta\eta'$, $\eta' \to \gamma\pi^+\pi^-$ estimated by the η' sidebands are 8.3% and 13.1%, respectively.

IV. PARTIAL WAVE ANALYSIS

After event selection, the numbers of remaining events for $J/\psi \to \gamma\eta\eta'$, $\eta' \to \eta\pi^+\pi^-$ and $J/\psi \to \gamma\eta\eta'$, $\eta' \to \gamma\pi^+\pi^-$

are 4788 and 10 544, respectively. The four-momenta of the reconstructed γ, η, and η' are used to perform the PWA fit.

A. Analysis method

Using the GPUPWA framework [51], a combined PWA fit is performed to the selected samples of $J/\psi \to \gamma\eta\eta'$, $\eta' \to \gamma\pi^+\pi^-$ and $J/\psi \to \gamma\eta\eta'$, $\eta' \to \eta\pi^+\pi^-$. Quasi two-body amplitudes in the sequential radiative decay processes $J/\psi \to \gamma X, X \to \eta\eta'$ and hadronic decay process $J/\psi \to \eta X, X \to \gamma\eta'$ and $J/\psi \to \eta'X, X \to \gamma\eta$ are constructed using the covariant tensor amplitudes described in Ref. [52]. Let A_X be the amplitude for a J/ψ decay process including intermediate resonance X. For J/ψ radiative decays, the general form of A_X is

$$A_X = \psi_\mu(m_1)e_\nu^*(m_2)\sum_k \Lambda_k U_k^{\mu\nu}, \qquad (1)$$

where the summation is over the number of independent amplitudes and for J/ψ hadronic decays, the general form of A_X is

$$A_X = \psi_\mu(m_1)\sum_k \Lambda_k U_k^\mu, \qquad (2)$$

where $\psi_\mu(m_1)$ is the polarization four-vector for the J/ψ; $e_\nu^*(m_2)$ is the polarization four-vector for the photon; m_1 and m_2 are the spin projections of the J/ψ and photon, respectively; $U_k^{\mu\nu}$ is the kth independent partial wave amplitude of J/ψ radiative decays to intermediate resonance X with coupling strength determined by a complex parameter Λ_k; and U_k^μ is the kth independent partial wave amplitude of J/ψ hadronic decays to intermediate resonance X with coupling strength determined by a complex parameter Λ_k. The partial wave amplitudes $U_k^{\mu\nu}$ and U_k^μ are constructed using the four-momenta of the reconstructed γ, η, η'.

The amplitudes for the J/ψ radiative decay processes $J/\psi \to \gamma f_0, \gamma f_2, \gamma f_4$ are given in Ref. [52]. For $J/\psi \to \gamma\eta_1$, where the η_1 is an isoscalar state with exotic quantum numbers $J^{PC} = 1^{-+}$, the η_1 can decay into $\eta\eta'$ in a P-wave [34,35] with two amplitudes:

$$U_{(\gamma\eta_1)1}^{\mu\nu} = g^{\mu\nu}p_\psi^\alpha\tilde{t}_\alpha^{(\eta_1)}f^{(\eta_1)}, \qquad (3)$$

$$U_{(\gamma\eta_1)2}^{\mu\nu} = q^\mu\tilde{t}^{(\eta_1)\nu}f^{(\eta_1)}, \qquad (4)$$

where $g^{\mu\nu}$ is the metric tensor, p_ψ is the four-momentum of the J/ψ, q is the four-momentum of the radiative photon, and $f^{(\eta_1)}$ is the propagator for the process $\eta_1 \to \eta\eta'$. Blatt-Weisskopf barrier factors [53–55] are included in the orbital angular momentum covariant tensors $\tilde{t}$. Due to the special properties (massless and gauge invariance) of the photon, the number of independent partial wave amplitudes for a

J/ψ radiative decay is smaller than for the corresponding decay to a massive vector meson, the details are given in Ref. [52].

For the J/ψ hadronic decay processes $J/\psi \to V\eta'$, $V \to \gamma\eta$, where V is vector meson that has quantum numbers $J^{PC} = 1^{--}$, such as ϕ, ρ, ω and their excitations, the corresponding amplitude is

$$U_{(V\eta')P}^{\mu\nu} = g^{\mu\mu'}\epsilon_{\mu'\nu'\alpha\beta}p_\psi^\alpha\tilde{T}_{(V\eta')}^\beta\epsilon^{\nu'\lambda\sigma\nu}q_\lambda p_{1\sigma}f^{(V)}, \qquad (5)$$

where, $\epsilon_{\mu'\nu'\alpha\beta}$ is the totally antisymmetric tensor, p_1 is the four-momentum of the η' from the J/ψ decay, $\tilde{T}_{V\eta'}^\beta$ is the orbital angular momentum covariant tensor of the process $J/\psi \to V\eta'$, and $f_{\gamma\eta}^{(V)}$ is the propagator for the process $V \to \gamma\eta$. The subscript P indicates $J/\psi \to V\eta'$ is in a P wave. The amplitude of $J/\psi \to V\eta, V \to \gamma\eta'$ is analogously to Eq. (5). For the process $J/\psi \to h_1\eta', h_1 \to \gamma\eta$, the corresponding two independent amplitudes are

$$U_{(h_1\eta')S}^{\mu\nu} = \tilde{g}_{(h_1)}^{\mu\nu}f^{(h_1)}, \qquad (6)$$

$$U_{(h_1\eta')D}^{\mu\nu} = \tilde{T}_{(h_1\eta')}^{(2)\mu\alpha}\tilde{g}_{(h_1)\alpha}^\nu f^{(h_1)}, \qquad (7)$$

where $\tilde{g}_{(h_1)}^{\mu\nu} = g^{\mu\nu} - \frac{p_{h_1}^\mu p_{h_1}^\nu}{p_{h_1}^2}$, p_{h_1} is the four-momentum of the h_1, and $f^{(h_1)}$ is the propagator for the process $h_1 \to \gamma\eta$. The superscript (2) on $\tilde{T}$ indicates the orbital momentum between h_1 and η' is 2. The subscripts S and D indicate $J/\psi \to h_1\eta'$ is in an S wave and D wave, respectively. The amplitudes for the process $J/\psi \to h_1\eta, h_1 \to \gamma\eta'$ are analogously to Eq. (6) and Eq. (7).

In this analysis, resonance decays are described by a Breit-Wigner (BW) function, parametrized by a constant-width, relativistic BW propagator,

$$f^{(X)} = \frac{1}{M^2 - s - \frac{1}{c^2}iM\Gamma}, \qquad (8)$$

where M and Γ are the mass and width of the intermediate resonance X, and $\sqrt{s}$ is the invariant mass of the $\eta\eta'$, $\gamma\eta$, or $\gamma\eta'$ system.

The complex coefficients of the amplitudes (relative magnitudes and phases) and resonance parameters (masses and widths) are determined by an unbinned maximum likelihood fit to the data. The likelihood is constructed following a method similar to that used in Ref. [56].

The probability to observe the ith event characterized by the measurement ξ_i, i.e., the measured four-momenta of the particles in the final state, is

$$P(\xi_i) = \frac{|M(\xi_i)|^2\epsilon(\xi_i)\Phi(\xi_i)}{\sigma'}, \qquad (9)$$

where $\epsilon(\xi_i)$ is the detection efficiency, $\Phi(\xi_i)$ is the standard element of phase space, and $M(\xi_i) = \sum_X A_X(\xi_i)$ is the matrix element describing the decay processes from the J/ψ to the final state $\gamma\eta\eta'$. $A_X(\xi_i)$ is the amplitude corresponding to intermediate resonance X as defined in Eq. (1) and Eq (2). $\sigma' \equiv \int |M(\xi)|^2 \epsilon(\xi)\Phi(\xi) d\xi$ is the normalization integral.

The joint probability for observing N events in the data sample is

$$\mathcal{L} = \prod_{i=1}^{N} \frac{|M(\xi_i)|^2 \epsilon(\xi_i)\Phi(\xi_i)}{\sigma'}. \qquad (10)$$

For technical reasons, rather than maximizing $\mathcal{L}$, $-\ln\mathcal{L}$ is minimized, with

$$-\ln\mathcal{L} = -\sum_{i=1}^{N} \ln |M(\xi_i)|^2 + N \ln \sigma'$$

$$-\sum_{i=1}^{N} \ln \epsilon(\xi_i)\Phi(\xi_i), \qquad (11)$$

for a given dataset. The third term is a constant and has no impact on the determination of the parameters of the amplitudes or on the relative changes of $-\ln\mathcal{L}$ values. In the fitting, the third term will not be considered.

The free parameters are optimized by MINUIT [57]. The normalization integral σ' is evaluated using MC with importance sampling [58,59]. An MC sample of N_{gen} is generated with signal events distributed uniformly in phase space. These events are put through the detector simulation, subjected to the selection criteria and yield a sample of N_{acc} accepted events. The normalization integral is computed as:

$$\sigma' = \int |M(\xi)|^2 \epsilon(\xi)\Phi(\xi) d\xi \propto \frac{1}{N_{\text{gen}}} \sum_{j}^{N_{\text{acc}}} |M(\xi_j)|^2, \qquad (12)$$

where the constant value of the phase space integral $\int \Phi(\xi) d\xi$ is ignored.

Instead of modeling the background, the likelihood is defined by the signal PDF [Eq. (11)] and the contribution to the negative log-likelihood from background events in the signal region is removed by subtracting out the negative

log-likelihood of events in the η' sideband region in proper proportion [60], i.e.,

$$-\ln\mathcal{L}_{\text{signal}} = -\left(\ln\mathcal{L}_{\text{data}} - \sum_i w_i \cdot \ln\mathcal{L}_{\text{background}}^i\right), \qquad (13)$$

where $-\ln\mathcal{L}_{\text{signal}}$ is the likelihood for the signal, $\ln\mathcal{L}_{\text{data}}$ is the likelihood calculated by Eq. (11) using the data sample, $\ln\mathcal{L}_{\text{background}}^i$ is the likelihood calculated by Eq. (11) using the events of ith sideband, and w_i is the normalization factor for background events in the ith sideband region, which is determined from the fit results of Figs. 1(a) and 1(b).

The number of fitted events N_X for an intermediate resonance X is defined as:

$$N_X = \frac{\sigma_X}{\sigma'} \cdot N, \qquad (14)$$

where N is the number of selected events after background subtraction, and

$$\sigma_X = \frac{1}{N_{\text{gen}}} \sum_{j}^{N_{\text{acc}}} |A_X(\xi_j)|^2, \qquad (15)$$

is calculated with the same MC sample as the normalization integral σ'.

The detection efficiency ϵ_X for an intermediate resonance X is obtained by the partial wave amplitude weighted MC sample,

$$\epsilon_X = \frac{\sum_{j}^{N_{\text{acc}}} |A_X(\xi_j)|^2}{\sum_{n}^{N_{\text{gen}}} |A_X(\xi_n)|^2}, \qquad (16)$$

A combined unbinned maximum likelihood fit is performed for the two decay channels by adding the negative log-likelihood of signal, $-\ln\mathcal{L}_{\text{signal}}$, for $J/\psi \to \gamma\eta\eta'$, $\eta' \to \eta\pi^+\pi^-$ and that for $J/\psi \to \gamma\eta\eta'$, $\eta' \to \gamma\pi^+\pi^-$ together. In the combined fit, the two decay modes share the same set of masses, widths, relative magnitudes, and phases.

The product branching fraction of $J/\psi \to \gamma X, X \to \eta\eta'$ is obtained according to:

$$\mathcal{B}(J/\psi \to \gamma X)\mathcal{B}(X \to \eta\eta') = \frac{N_{X_a} + N_{X_b}}{N_{J/\psi}(\epsilon_{X_a} \cdot \mathcal{B}(\eta' \to \eta\pi^+\pi^-)\mathcal{B}^2(\eta \to \gamma\gamma) + \epsilon_{X_b} \cdot \mathcal{B}(\eta' \to \gamma\pi^+\pi^-)\mathcal{B}(\eta \to \gamma\gamma))}, \qquad (17)$$

the subscript "a" and "b" indicate $J/\psi \to \gamma\eta\eta'$, $\eta' \to \eta\pi^+\pi^-$ and $J/\psi \to \gamma\eta\eta'$, $\eta' \to \gamma\pi^+\pi^-$, respectively; ϵ_{X_a} and ϵ_{X_b} are the detection efficiencies of the two different decay channels calculated by Eq. (16); $N_{J/\psi}$ is the total number

of J/ψ events; and $\mathcal{B}(\eta' \to \eta\pi^+\pi^-) = (42.5 \pm 0.5)\%$, $\mathcal{B}(\eta \to \gamma\gamma) = (39.41 \pm 0.20)\%$, $\mathcal{B}(\eta' \to \gamma\pi^+\pi^-) = (29.5 \pm 0.4)\%$ are the branching fractions taken from the PDG [14].

The product branching fraction of $J/\psi \to \eta X, X \to \gamma\eta'$ and $J/\psi \to \eta'X, X \to \gamma\eta$ can be calculated in a similar way to Eq. (17).

B. PWA results

To construct a set of two-body amplitudes to use in the PWA fit, a "PDG-optimized" set of amplitudes is first determined. To describe the $\eta\eta'$ and $\gamma\eta^{(\prime)}$ spectra, all kinematically allowed resonances with $J^{PC} = 0^{++}$, 2^{++}, and 4^{++} (for the $\eta\eta'$ system) and $J^{PC} = 1^{+-}$ and 1^{--} (for the $\gamma\eta^{(\prime)}$ systems) listed in the PDG [14] are considered. Within the allowed phase space (PHSP) of the $\eta\eta'$ system, four additional states [the $f_0(2102)$, $f_0(2330)$, $f_2(2240)$, and $f_4(2283)$] reported in Ref. [61] and an additional scalar state (the $f_0(1810)$) reported in Ref. [62] are also considered. Table I shows the complete set of resonances considered from the PDG, Ref. [61], and Ref. [62]. All possible sets of amplitudes corresponding to resonances listed in Table I are evaluated. The statistical significance for each resonance is determined by examining the probability of the change in negative log-likelihood values when this resonance is included or excluded in the fits, where the probability is calculated under the χ^2 distribution hypothesis taking into account the change in the number of degrees of freedom. The masses and widths of the resonances near $\eta\eta'$ mass threshold [$f_0(1500)$, $f_2(1525)$, $f_2(1565)$ and $f_2(1640)$] as well as those with small fit

TABLE I. The set of all intermediate resonances considered when the PDG-optimized set of amplitudes is developed. States with quantum numbers $J^{PC} = 0^{++}$, 2^{++}, and 4^{++} in the $\eta\eta'$ spectrum and states with quantum numbers $J^{PC} = 1^{+-}$ and 1^{--} in the $\gamma\eta^{(\prime)}$ spectra are considered.

Decay mode	0^{++}	2^{++}	4^{++}
$J/\psi \to \gamma X \to \gamma\eta\eta'$	$f_0(1500)$ $f_0(1710)$ $f_0(1810)$ [62] $f_0(2020)$ $f_0(2100)$ $f_0(2200)$ $f_0(2330)$ $f_0(2102)$ [61] $f_0(2330)$ [61]	$f_2(1525)$ $f_2(1565)$ $f_2(1640)$ $f_2(1810)$ $f_2(1910)$ $f_2(1950)$ $f_2(2010)$ $f_2(2150)$ $f_2(2220)$ $f_2(2300)$ $f_2(2340)$ $f_2(2240)$ [61]	$f_4(2050)$ $f_4(2300)$ $f_4(2283)$ [61]

	1^{--}	1^{+-}
$J/\psi \to \eta^{(\prime)}X \to \gamma\eta\eta'$	$\omega(1420)$ $\omega(1650)$ $\phi(1680)$ $\phi(2170)$ $\rho(1450)$ $\rho(1700)$ $\rho(1900)$	$h_1(1415)$ $h_1(1595)$

fractions ($<3\%$) are always fixed to the PDG [14] values. The mass and width of the $f_0(2330)$, which corresponds to a clear structure around 2.3 GeV/c^2 in the $\eta\eta'$ mass spectrum, are free parameters. All other masses and widths are also free parameters in the fit. The final PDG-optimized set of amplitudes is the combination where each included resonance has a statistical significance larger than 5σ. Results from the PWA fit using the PDG-optimized set of amplitudes, including the masses, the widths, and the statistical significances of each component, are shown in Table II, where the uncertainties are statistical only.

In the next step, a search is performed for additional resonances with $J^{PC} = 1^{-+}_{\eta\eta'}, 0^{++}_{\eta\eta'}, 2^{++}_{\eta\eta'}, 4^{++}_{\eta\eta'}, 1^{+-}_{\gamma\eta^{(\prime)}}$, and $1^{--}_{\gamma\eta^{(\prime)}}$, where the subscript labels the composition of the resonance, by individually adding each possibility to the PDG-optimized solution and scanning over its mass and width. The significance of each additional resonance at each mass and width is evaluated. The result indicates that a significant 1^{-+} contribution ($>7\sigma$) is needed around 1.9 GeV/c^2 in the $\eta\eta'$ system. The significances for all other additional contributions are less than 5σ. Therefore, an η_1 state is included in the PWA.

In the final step, a baseline set of amplitudes is determined by adding the η_1 state, with its mass and width as free parameters, to the PDG-optimized set of amplitudes. The statistical significances of all resonances in the PDG-optimized set are then reevaluated in the presence of the η_1 state. Contributions from the $f_0(2100)$, $h_1(1595)_{\gamma\eta'}$, $\rho(1700)_{\gamma\eta'}$, $\phi(2170)_{\gamma\eta}$, $f_2(1810)$, and $f_2(2340)$ in the PDG-optimized set of amplitudes become insignificant ($<3\sigma$) and are thus omitted from the baseline set of amplitudes, where the subscript labels the composition of the resonance. The statistical significance of the $f_4(2050)$ is reduced from 5.6σ to 4.6σ, but is still retained. By introducing the η_1, the mass and width of the $f_0(2020)$ becomes more consistent with the average values in the PDG [14]. In addition, a nonresonant contribution modeled by a 0^{++} $\eta\eta'$ system uniformly distributed in the phase space, is included with a significance of 15.7σ. After this amplitude selection process, the baseline set of amplitudes includes eleven components. The isoscalar state with exotic quantum numbers $J^{PC} = 1^{-+}$, the η_1, has a mass of $(1855 \pm 9_{\mathrm{stat}})$ MeV/c^2 and a width of $(188 \pm 18_{\mathrm{stat}})$ MeV with a statistical significance of 21.4σ. It is denoted as $\eta_1(1855)$.

The results of the PWA with the baseline set of amplitudes, including the masses and widths of the resonances, the product branching fractions $\mathcal{B}(J/\psi \to \gamma X)\mathcal{B}(X \to \eta\eta')$ and $\mathcal{B}(J/\psi \to \eta'X)\mathcal{B}(X \to \gamma\eta)$, and the statistical significances, are summarized in Table III. The fit fractions for each component and their interference fractions are shown in Table IV. The measured masses and widths of the $f_0(2020)$ and $f_2(2010)$ are consistent with the PDG [14] average values. The measured mass of the $f_0(2330)$, which is

TABLE II. The mass (M), width (Γ), PDG mass (M_{PDG}), PDG width (Γ_{PDG}), significance (Sig.) and the product branching fractions $\mathcal{B}(J/\psi \to \gamma X)\mathcal{B}(X \to \eta\eta')$, $\mathcal{B}(J/\psi \to \eta'X)\mathcal{B}(X \to \gamma\eta)$ and $\mathcal{B}(J/\psi \to \eta X)\mathcal{B}(X \to \gamma\eta')$ (B.F.) for each component in the PWA fit using the PDG-optimized set of amplitudes. The uncertainties are statistical.

Decay mode	Resonance	M (MeV/c^2)	Γ (MeV)	M_{PDG} (MeV/c^2)	Γ_{PDG} (MeV)	B.F. ($\times 10^{-5}$)	Sig.
$J/\psi \to \gamma X \to \gamma\eta\eta'$	$f_0(1500)$	1506	112	1506	112	3.05 ± 0.07	$\gg 30\sigma$
	$f_0(1810)$	1795	95	1795	95	0.07 ± 0.01	7.6σ
	$f_0(2020)$	1935 ± 5	266 ± 9	1992	442	1.67 ± 0.07	11.0σ
	$f_0(2100)$	2109 ± 11	253 ± 21	2086	284	0.33 ± 0.03	5.2σ
	$f_0(2330)$	2327 ± 4	44 ± 5	2314	144	0.07 ± 0.01	8.5σ
	$f_2(1565)$	1542	122	1542	122	0.20 ± 0.03	6.2σ
	$f_2(1810)$	1815	197	1815	197	0.37 ± 0.03	7.0σ
	$f_2(2010)$	2022 ± 6	212 ± 8	2011	202	1.36 ± 0.10	8.8σ
	$f_2(2340)$	2345	322	2345	322	0.25 ± 0.04	6.5σ
	$f_4(2050)$	2018	234	2018	234	0.11 ± 0.02	5.6σ
$J/\psi \to \eta' X \to \gamma\eta\eta'$	$h_1(1415)$	1416	90	1416	90	0.14 ± 0.01	10.3σ
	$h_1(1595)$	1584	384	1584	384	0.41 ± 0.04	9.7σ
	$\phi(2170)$	2160	125	2160	125	0.24 ± 0.03	5.6σ
$J/\psi \to \eta X \to \gamma\eta\eta'$	$h_1(1595)$	1584	384	1584	384	0.50 ± 0.03	11.0σ
	$\rho(1700)$	1720	250	1720	250	0.22 ± 0.03	8.8σ

TABLE III. The mass (M), width (Γ), PDG mass (M_{PDG}), PDG width (Γ_{PDG}), significance (Sig.) and the product branching fractions $\mathcal{B}(J/\psi \to \gamma X)\mathcal{B}(X \to \eta\eta')$ and $\mathcal{B}(J/\psi \to \eta'X)\mathcal{B}(X \to \gamma\eta)$ (B.F.) of each component in the PWA fit using the baseline set of amplitudes. The first uncertainties are statistical and the second are systematic.

Decay mode	Resonance	M (MeV/c^2)	Γ (MeV)	M_{PDG} (MeV/c^2)	Γ_{PDG} (MeV)	B.F. ($\times 10^{-5}$)	Sig.
	$f_0(1500)$	1506	112	1506	112	$1.81 \pm 0.11^{+0.19}_{-0.13}$	$\gg 30\sigma$
	$f_0(1810)$	1795	95	1795	95	$0.11 \pm 0.01^{+0.04}_{-0.03}$	11.1σ
	$f_0(2020)$	$2010 \pm 6^{+6}_{-4}$	$203 \pm 9^{+13}_{-11}$	1992	442	$2.28 \pm 0.12^{+0.29}_{-0.20}$	24.6σ
$J/\psi \to \gamma X \to \gamma\eta\eta'$	$f_0(2330)$	$2312 \pm 7^{+7}_{-3}$	$65 \pm 10^{+3}_{-12}$	2314	144	$0.10 \pm 0.02^{+0.01}_{-0.02}$	13.2σ
	$\eta_1(1855)$	$1855 \pm 9^{+6}_{-1}$	$188 \pm 18^{+3}_{-8}$	$\cdots$	$\cdots$	$0.27 \pm 0.04^{+0.02}_{-0.04}$	21.4σ
	$f_2(1565)$	1542	122	1542	122	$0.32 \pm 0.05^{+0.12}_{-0.02}$	8.7σ
	$f_2(2010)$	$2062 \pm 6^{+10}_{-7}$	$165 \pm 17^{+10}_{-5}$	2011	202	$0.71 \pm 0.06^{+0.10}_{-0.06}$	13.4σ
	$f_4(2050)$	2018	237	2018	237	$0.06 \pm 0.01^{+0.03}_{-0.01}$	4.6σ
	0^{++} PHSP	$\cdots$	$\cdots$	$\cdots$	$\cdots$	$1.44 \pm 0.15^{+0.10}_{-0.20}$	15.7σ
$J/\psi \to \eta' X \to \gamma\eta\eta'$	$h_1(1415)$	1416	90	1416	90	$0.08 \pm 0.01^{+0.01}_{-0.02}$	10.2σ
	$h_1(1595)$	1584	384	1584	384	$0.16 \pm 0.02^{+0.03}_{-0.01}$	9.9σ

TABLE IV. The fit fractions for each component and the interference fractions between two components(%) in the PWA fit with the baseline set of amplitudes. The uncertainties are statistical only.

Resonance	$f_0(1500)$	$f_0(1810)$	$f_0(2020)$	$f_0(2330)$	$h_1(1415)$	$h_1(1595)$	$\eta_1(1855)$	$f_2(1565)$	$f_2(2010)$	$f_4(2050)$	0^{++} PHSP
$f_0(1500)$	21.9 ± 1.4	-4.3 ± 0.4	16.2 ± 0.5	-1.0 ± 0.1	1.6 ± 0.2	-1.6 ± 0.9	0.2 ± 0.0	0.2 ± 0.1	0.6 ± 0.1	0.0 ± 0.0	13.4 ± 1.1
$f_0(1810)$		1.4 ± 0.1	-5.6 ± 0.6	0.4 ± 0.0	-0.1 ± 0.0	0.6 ± 0.1	0.0 ± 0.0	-0.2 ± 0.0	0.1 ± 0.0	0.0 ± 0.0	2.0 ± 0.3
$f_0(2020)$			29.5 ± 1.6	-3.7 ± 0.5	0.0 ± 0.2	-3.6 ± 0.4	0.2 ± 0.0	1.1 ± 0.1	0.1 ± 0.1	0.1 ± 0.0	-15.9 ± 1.8
$f_0(2330)$				1.4 ± 0.2	0.1 ± 0.0	0.3 ± 0.1	0.0 ± 0.0	-0.1 ± 0.0	-0.2 ± 0.0	0.0 ± 0.0	2.6 ± 0.3
$h_1(1415)$					1.1 ± 0.2	-1.1 ± 0.3	-0.2 ± 0.1	0.1 ± 0.1	0.2 ± 0.1	0.0 ± 0.0	2.3 ± 0.3
$h_1(1595)$						2.1 ± 0.3	0.5 ± 0.1	-0.3 ± 0.3	0.0 ± 0.2	0.1 ± 0.0	2.3 ± 1.0
$\eta_1(1855)$							3.5 ± 0.5	0.0 ± 0.0	-0.1 ± 0.0	0.0 ± 0.0	0.1 ± 0.0
$f_2(1565)$								4.6 ± 0.7	-0.6 ± 0.8	0.0 ± 0.0	-0.9 ± 0.1
$f_2(2010)$									10.2 ± 0.8	-0.1 ± 0.1	0.2 ± 0.1
$f_4(2050)$										0.8 ± 0.2	0.0 ± 0.0
0^{++} PHSP											18.5 ± 1.9

unestablished in the PDG [14], is consistent with the results of Ref. [61], but our measured width is 79 MeV smaller (3.4σ).

All other resonances considered have statistical significance less than 3σ when added to the baseline set of amplitudes, as shown in Table V. To investigate additional possible contributions, resonances with different J^{PC} ($0^{++}_{\eta\eta'}$, $1^{-+}_{\eta\eta'}$, $2^{++}_{\eta\eta'}$, $4^{++}_{\eta\eta'}$, $1^{+-}_{\gamma\eta^{(\prime)}}$, and $1^{--}_{\gamma\eta^{(\prime)}}$.) and with different masses and widths are added to the baseline set of amplitudes. No significant contributions from additional resonances with conventional quantum numbers are found. The most significant additional contribution (4.4σ) comes from an exotic 1^{-+} component around 2.2 GeV. Changing the J^{PC} assignment of the 0^{++} PHSP component in the baseline set of amplitudes to $1^{-+}_{\eta\eta'}$, $2^{++}_{\eta\eta'}$, $4^{++}_{\eta\eta'}$, $1^{+-}_{\gamma\eta^{(\prime)}}$, and $1^{--}_{\gamma\eta^{(\prime)}}$,

TABLE V. Additional resonances considered, their J^{PC}, the change in negative log-likelihood ($\Delta \ln \mathcal{L}$) when each is added to the baseline set of amplitudes, the change in the number of free parameters (Δdof), and the resulting statistical significance (Sig.).

Decay mode	Resonance	J^{PC}	$\Delta \ln \mathcal{L}$	Δdof	Sig.
$J/\psi \to \gamma X \to \gamma\eta\eta'$	$f_2(1525)$	2^{++}	6.3	6	1.9σ
	$f_2(1810)$	2^{++}	2.7	6	0.7σ
	$f_0(1710)$	0^{++}	3.4	2	2.1σ
	$f_2(1910)$	2^{++}	3.9	6	1.1σ
	$f_2(1950)$	2^{++}	2.6	6	0.6σ
	$f_0(2100)$	0^{++}	1.1	2	1.1σ
	$f_2(2150)$	2^{++}	2.3	6	0.5σ
	$f_0(2200)$	0^{++}	0.4	2	0.4σ
	$f_2(2220)$	2^{++}	8.6	6	2.6σ
	$f_2(2300)$	2^{++}	7.2	6	2.2σ
	$f_4(2300)$	4^{++}	2.3	6	0.5σ
	$f_0(2330)$	0^{++}	1.5	2	1.2σ
	$f_2(2340)$	2^{++}	6.3	6	1.9σ
	$f_0(2102)$ [61]	0^{++}	0.1	2	0.2σ
	$f_2(2240)$ [61]	2^{++}	2.9	6	0.7σ
	$f_2(2293)$ [61]	2^{++}	4.1	6	1.2σ
	$f_4(2283)$ [61]	4^{++}	0.9	6	0.1σ
$J/\psi \to \eta' X \to \gamma\eta\eta'$	$\rho(1450)$	1^{--}	3.4	2	2.1σ
	$\rho(1700)$	1^{--}	0.8	2	0.7σ
	$\rho(1900)$	1^{--}	0.0	2	0σ
	$\omega(1420)$	1^{--}	5.3	2	2.8σ
	$\omega(1650)$	1^{--}	2.6	2	1.7σ
	$\phi(1680)$	1^{--}	4.3	2	2.5σ
	$\phi(2170)$	1^{--}	0.4	2	0.4σ
$J/\psi \to \eta X \to \gamma\eta\eta'$	$h_1(1415)$	1^{+-}	1.3	4	0.5σ
	$h_1(1595)$	1^{+-}	8.1	4	2.9σ
	$\rho(1450)$	1^{--}	1.3	2	1.1σ
	$\rho(1700)$	1^{--}	3.1	2	2.0σ
	$\rho(1900)$	1^{--}	6.1	2	3.0σ
	$\omega(1420)$	1^{--}	2.5	2	1.7σ
	$\omega(1650)$	1^{--}	0.8	2	0.7σ
	$\phi(1680)$	1^{--}	2.1	2	1.5σ
	$\phi(2170)$	1^{--}	0.1	2	0.1σ

results in a worse negative log-likelihood by at least 57. Furthermore, additional non-resonant contributions with all other J^{PC} assignments are found to be insignificant.

Figures 2(a)–2(c) show the invariant mass distributions of $M(\eta\eta')$, $M(\gamma\eta)$, and $M(\gamma\eta')$ for the data (with background subtracted) and the PWA fit projections, respectively. Figure 2(d) shows the $\cos\theta_\eta$ distribution, where θ_η is the angle of the η momentum in the $\eta\eta'$ (Jacob and Wick) helicity frame (in which the $\eta\eta'$ system is at rest and the z-axis is defined by the momentum of the photon) [63]. This angle carries information about the spin of the particle decaying to $\eta\eta'$. The $\chi^2/n_{\rm bin}$ value is displayed on each figure to demonstrate the goodness of fit, where $n_{\rm bin}$ is the number of bins in each histogram, and χ^2 is defined as:

$$\chi^2 = \sum_{i=1}^{n_{\rm bin}} \frac{(n_i - v_i)^2}{v_i}, \tag{18}$$

where n_i and v_i are the number of events for the data and the fit projections with the baseline set of amplitudes in the ith bin of each figure, respectively. In comparison, the $\chi^2/n_{\rm bin}$ values for the PDG-optimized set of amplitudes for the distributions of $M(\eta\eta')$, $M(\gamma\eta)$, $M(\gamma\eta')$, and $\cos\theta_\eta$ are 0.26, 0.43, 0.12 and 0.30 worse than baseline set of amplitudes, respectively. Figure 3 shows the Dalitz plots for the PWA fit projection from the baseline set of amplitudes, the selected data, and the background estimated from the η' sideband. Figures 2 and 3 indicates that the data and the PWA fit result (baseline set of amplitudes) are in good agreements. Compared with the PDG-optimized set, the negative log-likelihood value of the baseline set is improved by 32 units and the number of free parameters is reduced by 16.

C. Further checks on the $\eta_1(1855)$

Various checks are performed to validate the existence of the $\eta_1(1855)$. The fits are carried out by assigning all other possible J^{PC} to the $\eta_1(1855)$, and the negative log-likelihoods are worse by at least 235 units (21.8σ). To probe the significance of the BW phase motion, the BW parameterization of the $\eta_1(1855)$ in the baseline PWA is replaced with an amplitude whose magnitude matches that of a BW function but with constant phase (independent of s). This alternative fit has a negative log-likelihood 43 units (9.2σ) worse than the baseline fit, which indicates that a resonant structure is favorable. In the scenario $\eta_1(1855)$ is removed from the baseline set of amplitudes, the significance of $\eta_1(1855)$ with different masses and widths are evaluated. The changes of negative log-likelihood value are shown in Fig. 4. The result shows that a significant 1^{-+} contribution is needed around 1.85 GeV/c^2.

To visualize the agreement between the PWA fit results and data, angular moments as a function of $M(\eta\eta')$ can be calculated for data (with background subtracted) and the PWA model. For events within a given region of $M(\eta\eta')$,
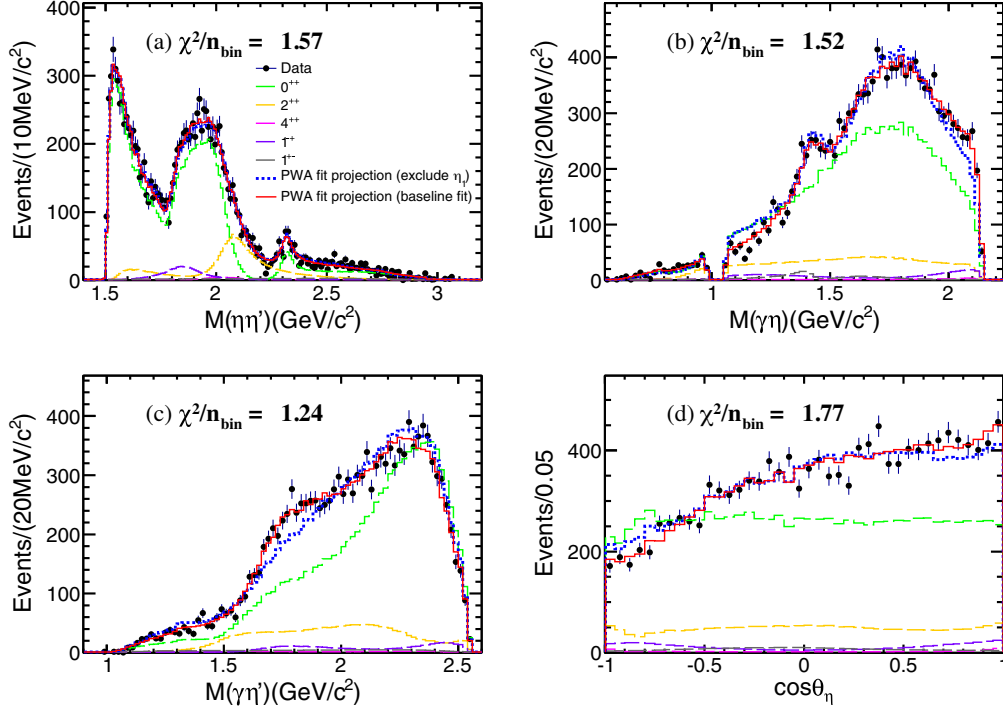
FIG. 2. Background-subtracted data (black points) and the PWA fit projections (lines) for (a,b,c) the invariant mass distributions of (a) $\eta\eta'$, (b) $\gamma\eta$, and (c) $\gamma\eta'$, and (d) the distribution of $\cos\theta_\eta$, where θ_η is the angle of the η momentum in the $\eta\eta'$ helicity coordinate system. The red lines are the total fit projections from the baseline PWA. The blue lines are the total fit projections from a fit excluding the η_1 component. The dashed lines for the $1^{-+}, 0^{++}, 2^{++}, 4^{++}$ and 1^{+-} contributions are the coherent sums of amplitudes for each J^{PC}.
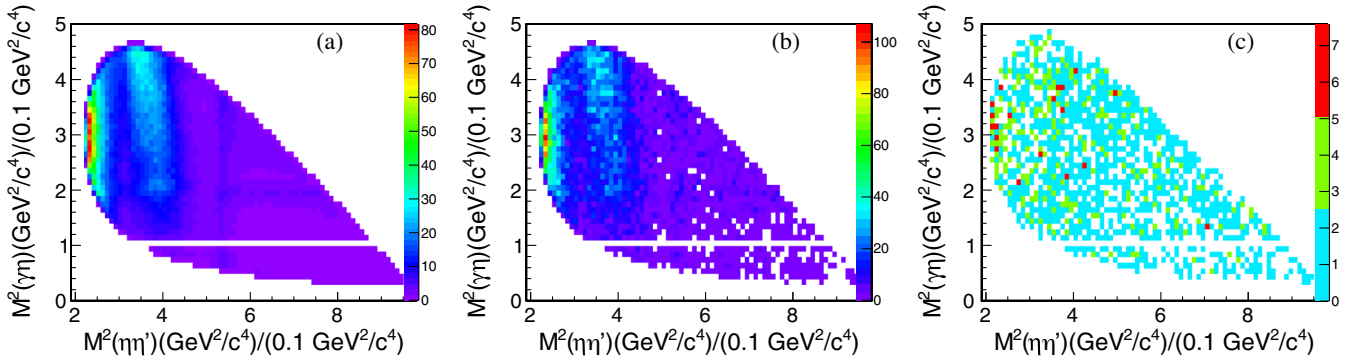

FIG. 3. Dalitz plots for (a) the baseline PWA, (b) the selected data, and (c) background estimated from the η' sideband.

the $\cos\theta_\eta$ distribution can be expressed as an expansion in terms of Legendre polynomials. The coefficients, which are called the unnormalized moments of the expansion, characterize the spin of the contributing $\eta\eta'$ resonances. The moment for the kth bin of $M(\eta\eta')$ is

$$\langle Y_l^0 \rangle \equiv \sum_{i=1}^{N_k} W_i Y_l^0(\cos\theta_\eta^i). \tag{19}$$

For data, N_k is the number of observed events in the kth bin of $M(\eta\eta')$ and W_i is a weight used to implement background subtraction. For the PWA model, N_k is the number

of events in a PHSP MC sample, which is generated with signal events distributed uniformly in phase space, and W_i is the intensity for each event calculated in the PWA model.

Neglecting $\eta\eta'$ amplitudes with spin greater than 2, and ignoring the effects of symmetrization and the presence of resonance contributions in the $\gamma\eta$ and $\gamma\eta'$ subsystems, the moments are related to the spin-0 (S), spin-1 (P) and spin-2 (D) amplitudes by [64]:

$$\sqrt{4\pi}\langle Y_0^0 \rangle = S^2 + P^2 + D^2, \tag{20}$$

$$\sqrt{4\pi}\langle Y_1^0 \rangle = 2SP\cos\phi_P + 4PD\cos(\phi_P - \phi_D), \tag{21}$$
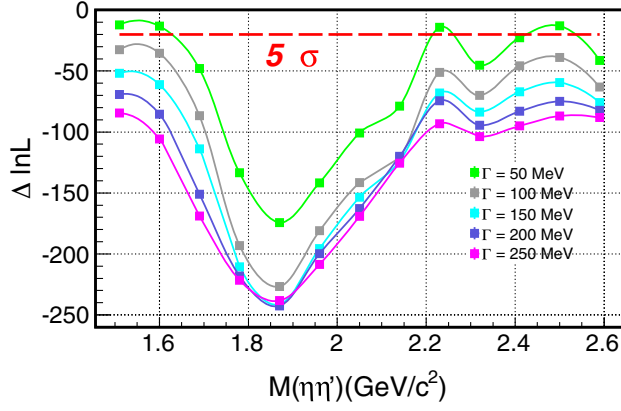
FIG. 4.   The change in negative log-likelihood values for a range of η_1 resonance parameters in the baseline set of amplitudes. The red dashed line indicates that the statistical significances of the hypotheses under the red dashed line are higher than 5σ.

$$\sqrt{4\pi}\langle Y_2^0\rangle = \frac{2}{\sqrt{5}}P^2 + \frac{2\sqrt{5}}{7}D^2 + 2SD\cos\phi_D, \qquad (22)$$

$$\sqrt{4\pi}\langle Y_3^0\rangle = \frac{6}{5}\sqrt{\frac{15}{7}}PD\cos(\phi_P - \phi_D), \qquad (23)$$

$$\sqrt{4\pi}\langle Y_4^0\rangle = \frac{6}{7}D^2, \qquad (24)$$

where ϕ_P and ϕ_D are the phases of the P wave and D wave relative to the S wave. Figure 5 shows the moments computed for the data and the PWA model, using Eq. (19), where good data/PWA consistency can be seen. The need for the $\eta_1(1855)$ P-wave component is apparent in the $\langle Y_1^0\rangle$ moment [Fig. 5(b)].
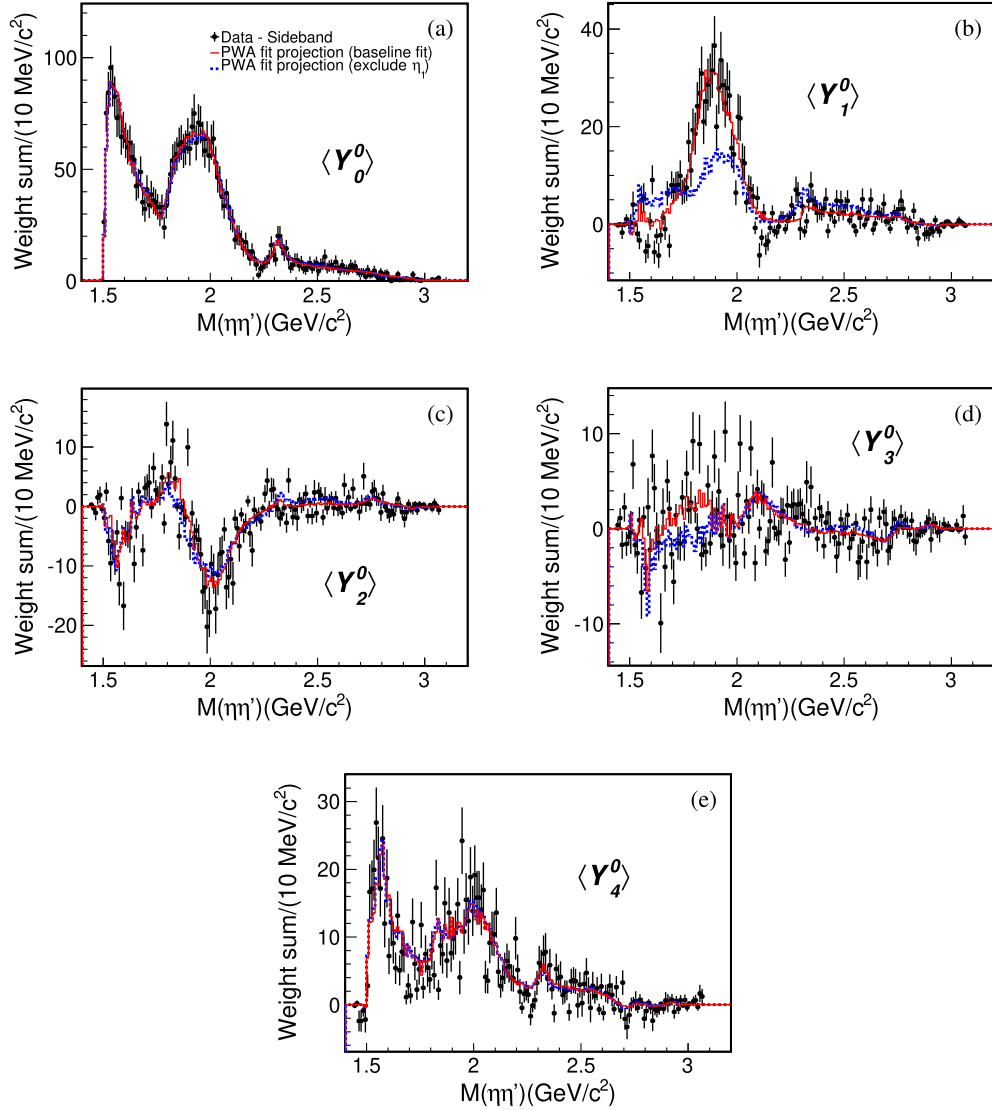
FIG. 5.   The distributions of the unnormalized moments $\langle Y_L^0\rangle$ ($L = 0, 1, 2, 3$ and 4) for $J/\psi \to \gamma\eta\eta'$ as functions of the $\eta\eta'$ mass. Black dots with error bars represent the background-subtracted data weighted with angular moments; the red solid lines represent the baseline fit projections; and the blue dotted lines represent the projections from a fit excluding the η_1 component.
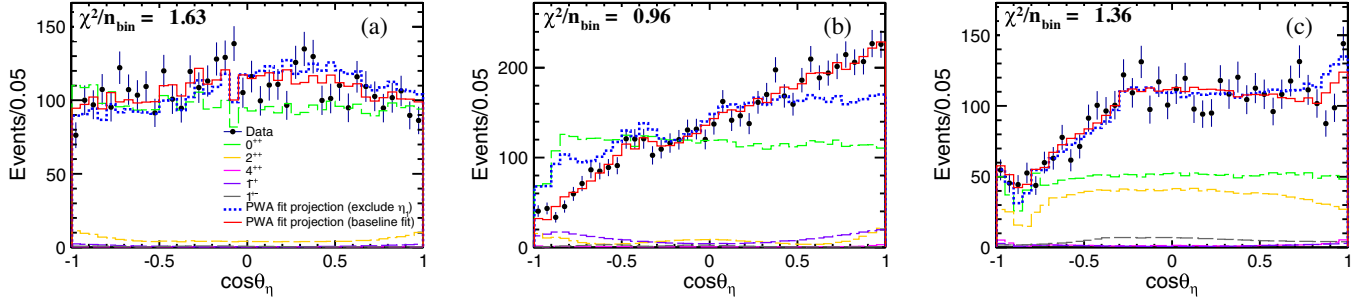
FIG. 6. Background-subtracted data (black points) and the PWA fit projections (lines) for the $\cos\theta_\eta$ distribution when the $\eta\eta'$ mass is restricted to the regions: (a) [1.5,1.7], (b) [1.7,2.0], and (c) [2.0, 3.2] GeV/c^2. The red lines are the total fit projections from the baseline PWA. The blue lines are the total fit projections from a fit excluding the η_1 component.

Figure 6 shows a comparison of the data and the PWA projection of $\cos\theta_\eta$ in different $M(\eta\eta')$ regions ([1.5,1.7], [1.7,2.0] and [2.0, 3.2] GeV/c^2). There is a clear asymmetry in the $\cos\theta_\eta$ distribution in the region [1.7, 2.0] GeV/c^2 largely due to the $\eta_1(1855)$ signal, and the $\chi^2/n_{\rm bin}$ of this region indicates a good agreement between data and the fitting results.

D. Discussion of the $f_0(1500)$ and $f_0(1710)$

The dominant contributions in the baseline PWA are from the scalar resonances. A significant signal for the $f_0(1500)$ is observed with a large product branching fraction $(\mathcal{B}(J/\psi \to \gamma f_0(1500)) \quad \mathcal{B}(f_0(1500) \to \eta\eta') = (1.81 \pm 0.11_{\rm stat}) \times 10^{-5})$. Since the mass of the $f_0(1500)$ is close to the $\eta\eta'$ mass threshold and the $f_0(1500)$ has other decay modes, we parameterize the $f_0(1500)$ with a Flatté-like form with its mass and width as free parameters. The Flatté-like propagator is

$$f^{(f_0(1500))}_{\rm Flatt\acute{e}} = \frac{1}{M^2 - s - \frac{1}{c^2}i\sqrt{s}\Gamma(s)}, \qquad (25)$$

$$\Gamma(s) = g\Gamma\left(\frac{M^2}{s}\right)\left(\frac{\rho(s)}{\rho(M^2)}\right)^{2l+1} + (1-g)\Gamma_0, \quad (26)$$

where the Γ in the first term of $\Gamma(s)$ is an effective parameter corresponds to the decay mode $f_0(1500)\to\eta\eta'$, l is orbital angular momentum of $\eta\eta'$ system, g is $\mathcal{B}(f_0(1500) \to \eta\eta')$, which is estimated to be 0.02 from the PDG [14], the second term corresponds to all other decay modes of the $f_0(1500)$, and Γ_0 is a constant which represents the total width of the $f_0(1500)$ listed in the PDG [14]. $\rho(s)$ is the momentum magnitude of $\eta^{(\prime)}$ in the $\eta\eta'$ rest frame:

$$\rho(s) = \sqrt{\frac{((s + s_\eta - s_{\eta'})^2}{4s} - s_{\eta'}}. \qquad (27)$$

The impact of using the Flatté-like parametrization for the $f_0(1500)$ is assigned as a systematic uncertainty, which is discussed further in Sec. V.

The ratio $\mathcal{B}(f_0 \to \eta\eta')/\mathcal{B}(f_0 \to \pi\pi)$ can be calculated with the branching fractions measured in this analysis and in $J/\psi \to \gamma\pi^+\pi^-$, $\gamma\pi^0\pi^0$ [65]. The ratio $\mathcal{B}(f_0(1500) \to \eta\eta')/\mathcal{B}(f_0(1500) \to \pi\pi)$ is determined to be $(8.96 \pm 2.80_{\rm stat}) \times 10^{-2}$, where the uncertainty is statistical only. In comparison, the product branching fraction $\mathcal{B}(J/\psi \to \gamma f_0(1810))\mathcal{B}(f_0(1810) \to \eta\eta')$ is $(0.11 \pm 0.01_{\rm stat}) \times 10^{-5}$. If we consider the $f_0(1810)$ and $f_0(1710)$ to be the same state, the ratio $\mathcal{B}(f_0(1810) \to \eta\eta')/\mathcal{B}(f_0(1710) \to \pi\pi)$ is $(1.39^{+0.62}_{-0.52}) \times 10^{-2}$, where the error includes both the systematic and statistical uncertainties. If the $f_0(1710)$ is added to the baseline set of amplitudes, the statistical significance of the $f_0(1710)$ is 2.1σ, the $\mathcal{B}(J/\psi \to \gamma f_0(1710))\mathcal{B}(f_0(1710) \to \eta\eta')$ is $(1.87 \pm 0.54_{\rm stat}) \times 10^{-7}$, and the $\mathcal{B}(J/\psi \to \gamma f_0(1500))\times \mathcal{B}(f_0(1500) \to \eta\eta')$ becomes $(1.98 \pm 0.06_{\rm stat}) \times 10^{-5}$. If the $f_0(1810)$ is replaced by the $f_0(1710)$ with mass and width taken from the PDG, the product branching fraction $\mathcal{B}(J/\psi\to\gamma f_0(1710))\mathcal{B}(f_0(1710)\to\eta\eta')$ becomes $(7.16 \pm 2.21_{\rm stat}) \times 10^{-7}$ and the negative log-likelihood is worse by 29 units (7.3σ). There is therefore no significant evidence for $J/\psi \to \gamma f_0(1710) \to \gamma\eta\eta'$. To determine the upper limits on $\mathcal{B}(J/\psi \to \gamma f_0(1710))\mathcal{B}(f_0(1710) \to \eta\eta')$ for different scenarios, the same approach as that in Ref. [66] is used. For each alternative fit, the upper limit is determined at 90% of the integral of a Gaussian distribution with mean and width equal to the fitting yield and the statistical uncertainty. The maximum value is taken as the upper limit.

V. SYSTEMATIC UNCERTAINTIES

The sources of systematic uncertainty are divided into two categories. The first category concerns the systematic uncertainties related to event selection, which are applicable to measurements of the branching fractions. These sources of systematic uncertainties are described below.

The second category of systematic uncertainties concerns the PWA and will be treated later.

(i) Pion tracking. The MDC tracking efficiency of charged pions is investigated using a clean control sample of $J/\psi \to p\bar{p}\pi^+\pi^-$ [67]. The difference in tracking efficiency between data and MC simulation is 1% for each charged pion.

(ii) Photon detection efficiency. The photon detection efficiency is studied with a clean sample of $J/\psi \to \rho^0\pi^0$ [68]. The result shows that the data-MC efficiency difference is 1% per photon.

(iii) Kinematic fit. To investigate the systematic uncertainty associate with the kinematic fit, the track helix parameter correction method [69] is used. The difference in the detection efficiency between using and not using the helix correction is taken as the systematic uncertainty.

(iv) η' mass resolution. The difference in the mass resolution between data and MC simulation leads to uncertainties related to the η' mass window requirement. This is investigated by smearing the MC simulation to improve the consistency between data and MC simulation. The difference of the detection efficiency before and after smearing is assigned as the systematic uncertainty for the η' mass window requirement.

(v) Other systematic uncertainties. The systematic uncertainty due to the number of J/ψ events is determined to be 0.43% according to Ref. [37]. The uncertainties on the intermediate decay branching fractions of $\eta' \to \eta\pi^+\pi^-$, $\eta' \to \gamma\pi^+\pi^-$, and $\eta \to \gamma\gamma$ are taken from the world average values [14], which are 0.5%, 0.4% and 0.2%, respectively.

For the two η' decay modes, the systematic uncertainties from pion tracking, four photon detection, number of J/ψ events, $\mathcal{B}(\eta \to \gamma\gamma)$ are common systematic uncertainties and the other systematic uncertainties are independent systematic uncertainties. The combination of common and independent systematic uncertainties for these two decay modes are calculated with the weighted least squares method [70], and the total systematic uncertainty is determined to be 4.8%. A summary of all systematic uncertainties related to event selection is shown in Table VI.

Systematic uncertainties from the PWA impact the branching fractions and resonance parameters. These are studied below, and the statistical significance of the $\eta_1(1855)$ is recalculated in every variation.

(i) BW parametrization. Uncertainty from the BW parametrization is estimated by the changes in the fit result caused by replacing the constant width Γ_0 of the BW for the threshold state $f_0(1500)$ with a mass dependent width as described in Sec. IV D. The statistical significance of the $\eta_1(1855)$ in this case is 21.8σ.

TABLE VI. Relative systematic uncertainties related to event selection for the determination of the branching fraction (in %).

Common systematic uncertainties		
Sources	$\eta' \to \eta\pi^+\pi^-$	$\eta' \to \gamma\pi^+\pi^-$
Pion tracking		2
Four photon detection		4
Number of J/ψ events		0.43
$\mathcal{B}(\eta \to \gamma\gamma)$		0.2
Total		4.5

Independent systematic uncertainties		
Sources	$\eta' \to \eta\pi^+\pi^-$	$\eta' \to \gamma\pi^+\pi^-$
Another photon detection	1	$\cdots$
Kinematic fit	1.5	2.6
η' mass resolution	0.3	0.2
$\mathcal{B}(\eta' \to \eta\pi^+\pi^-)$	0.5	$\cdots$
$\mathcal{B}(\eta' \to \gamma\pi^+\pi^-)$	$\cdots$	0.4
$\mathcal{B}(\eta \to \gamma\gamma)$ for another one	0.2	$\cdots$
Total	1.9	2.6
Combined result		4.8

(ii) Uncertainty from resonance parameters. In the baseline fit, the resonance parameters of the $f_0(1500)$, $f_2(1565)$, $f_4(2050)$, $h_1(1415)_{\gamma\eta}$, and $h_1(1595)_{\gamma\eta}$ are fixed to PDG [14] average values, and the resonance parameters of $f_0(1810)$ are fixed to the previous measurment [62]. An alternative fit is performed where resonance parameters are allowed to vary within one standard deviation of the PDG values [14] and Ref. [62], and the changes in the results are taken as systematic uncertainties. The statistical significance of the $\eta_1(1855)$ in this case is 20.6σ.

(iii) Background uncertainty. To estimate the uncertainty due to the background estimation, alternative fits are performed using different η' sideband regions and different background normalization factors. In detail, the background normalization factors are varied by one standard deviation, which is determined from the fit results of Figs. 1(a) and 1(b). The statistical significance of the $\eta_1(1855)$ is always above 21.1σ. The changes in the branching fractions and resonance parameters are assigned as systematic uncertainties.

(iv) Uncertainty from additional resonances. Uncertainties arising from possible additional resonances are estimated by adding the $f_0(1710)$, $f_2(2220)$, $f_4(2300)$, $h_1(1595)_{\gamma\eta'}$, and $\rho(1900)_{\gamma\eta'}$, which are the most significant additional resonances for each possible J^{PC}, into the baseline fit individually. The resulting changes in the measurements are assigned as systematic uncertainties. With the addition of the $f_0(1710)$, $f_2(2220)$, $f_4(2300)$,

TABLE VII. Systematic uncertainties on the masses (in MeV/c^2) and widths (in MeV) of the $f_0(2020)$, $f_0(2330)$, $\eta_1(1855)$, and $f_2(2010)$, denoted as ΔM and $\Delta\Gamma$, respectively.

Sources	$f_0(2020)$		$f_0(2330)$		$\eta_1(1855)$		$f_2(2010)$	
	ΔM	$\Delta\Gamma$	ΔM	$\Delta\Gamma$	ΔM	$\Delta\Gamma$	ΔM	$\Delta\Gamma$
Breit-Wigner formula	$^{+0}_{-1}$	$^{+10}_{-0}$	$^{+0}_{-1}$	$^{+1}_{-0}$	$^{+0}_{-1}$	$^{+2}_{-0}$	$^{+0}_{-4}$	$^{+3}_{-0}$
Resonance parameters	$^{+1}_{-0}$	$^{+0}_{-10}$	$^{+0}_{-3}$	$^{+2}_{-0}$	$^{+2}_{-0}$	$^{+0}_{-1}$	$^{+0}_{-0}$	$^{+0}_{-2}$
Extra resonances	$^{+4}_{-2}$	$^{+9}_{-2}$	$^{+7}_{-0}$	$^{+1}_{-9}$	$^{+4}_{-0}$	$^{+1}_{-6}$	$^{+10}_{-5}$	$^{+10}_{-0}$
Background uncertainty	$^{+0}_{-1}$	$^{+0}_{-4}$	$^{+3}_{-0}$	$^{+1}_{-7}$	$^{+3}_{-0}$	$^{+1}_{-5}$	$^{+0}_{-1}$	$^{+0}_{-5}$
Total	$^{+4}_{-3}$	$^{+13}_{-11}$	$^{+7}_{-3}$	$^{+3}_{-12}$	$^{+6}_{-1}$	$^{+3}_{-8}$	$^{+10}_{-7}$	$^{+10}_{-5}$

TABLE VIII. Relative systematic uncertainties on the branching fractions of $J/\psi \to \gamma X \to \gamma\eta\eta'$ or $J/\psi \to \eta^{(\prime)} X \to \gamma\eta\eta'$ (relative uncertainties, in %).

Sources	$f_0(1500)$	$f_0(1810)$	$f_0(2020)$	$f_0(2330)$	$\eta_1(1855)$	$f_2(1565)$	$f_2(2010)$	$f_4(2050)$	0^{++} PHSP	$h_1(1415)$	$h_1(1595)$
Event selection						$^{+4.8}_{-4.8}$					
Breit-Wigner formula	$^{+0}_{-1.7}$	$^{+11.6}_{-0}$	$^{+6.9}_{-0}$	$^{+3.2}_{-0}$	$^{+0}_{-1.1}$	$^{+17.8}_{-0}$	$^{+0.2}_{-0}$	$^{+4.2}_{-0}$	$^{+0}_{-0.6}$	$^{+0}_{-8.2}$	$^{+0}_{-4.1}$
Extra resonances	$^{+9.4}_{-1.0}$	$^{+30.4}_{-8.4}$	$^{+10.0}_{-0}$	$^{+7.8}_{-13.4}$	$^{+3.5}_{-10.4}$	$^{+31.5}_{-2.7}$	$^{+12.9}_{-6.5}$	$^{+44.4}_{-4.7}$	$^{+5.1}_{-12.2}$	$^{+11.0}_{-9.1}$	$^{+16.2}_{-2.2}$
Resonance parameters	$^{+0}_{-4.8}$	$^{+0}_{-25.6}$	$^{+0}_{-6.5}$	$^{+3.6}_{-0}$	$^{+0}_{-6.1}$	$^{+5.5}_{-0}$	$^{+0.2}_{-0}$	$^{+0}_{-1.4}$	$^{+0}_{-4.6}$	$^{+0}_{-11.4}$	$^{+0}_{-4.3}$
Background uncertainty	$^{+0.5}_{-0.6}$	$^{+0.4}_{-7.5}$	$^{+0.8}_{-3.4}$	$^{+0.3}_{-10.4}$	$^{+0.2}_{-1.1}$	$^{+11.0}_{-0}$	$^{+0}_{-2.7}$	$^{+31.9}_{-6.5}$	$^{+0}_{-1.8}$	$^{+0}_{-8.8}$	$^{+8.4}_{-0.6}$
Total	$^{+10.6}_{-7.1}$	$^{+32.9}_{-28.4}$	$^{+13.1}_{-8.8}$	$^{+10.3}_{-17.6}$	$^{+5.9}_{-13.1}$	$^{+38.5}_{-5.5}$	$^{+13.7}_{-8.5}$	$^{+55.0}_{-9.5}$	$^{+7.0}_{-14.0}$	$^{+12.0}_{-19.5}$	$^{+18.8}_{-8.0}$

$h_1(1595)_{\gamma\eta'}$, and $\rho(1900)_{\gamma\eta'}$, the statistical significances of the $\eta_1(1855)$ are 22.1σ, 21.2σ, 21.1σ, 19.0σ, and 21.1σ, respectively.

For each alternative fit performed to estimate the systematic uncertainties in the PWA fit procedure, the changes of the measurements are taken as the one-sided systematic uncertainties. For each measurement, the individual uncertainties are assumed to be independent and are added in quadrature to obtain the total systematic uncertainty on the negative and positive sides, respectively. The sources of systematic uncertainties affecting the measurements of masses and widths of the $f_0(2020)$, $f_0(2330)$, $\eta_1(1855)$, $f_2(2010)$ and their contributions are summarized in Table VII. The relative systematic uncertainties relevant to the branching fraction measurements are summarized in Table VIII.

Including the systematic uncertainties, the ratio $\mathcal{B}(f_0(1500) \to \eta\eta')/\mathcal{B}(f_0(1500) \to \pi\pi)$ is measured to be $(8.96^{+2.95}_{-2.87}) \times 10^{-2}$, where the error includes both the systematic and statistical uncertainties. To include the systematic uncertainties in the upper limit $\mathcal{B}(f_0(1710) \to \eta\eta')/\mathcal{B}(f_0(1710) \to \pi\pi)$, the additive systematic uncertainties, i.e., the systematic uncertainties on the upper limit associated with the PWA, are considered by performing alternative fits and taking the maximum value as the upper limit. The multiplicative systematic uncertainties, i.e. the other systematic uncertainties, are taken into account by

dividing by the factor $(1 - \delta_{\text{combined}})$, where δ_{combined} is the systematic uncertainties associated with the event selection and the uncertainty of branching fractions and the uncertainty of $J/\psi \to \gamma f_0(1710) \to \gamma\pi\pi$ [65]. The upper limit on $\mathcal{B}(f_0(1710) \to \eta\eta')/\mathcal{B}(f_0(1710) \to \pi\pi)$ at 90% CL is determined to be 1.61×10^{-3}.

VI. SUMMARY

In summary, a PWA of $J/\psi \to \gamma\eta\eta'$ has been performed based on $(10.09 \pm 0.04) \times 10^9$ J/ψ events collected with the BESIII detector. An isoscalar state with exotic quantum numbers $J^{PC} = 1^{-+}$, denoted as $\eta_1(1855)$, has been observed for the first time. Its mass and width are measured to be $(1855 \pm 9^{+6}_{-1})$ MeV/c^2 and $(188 \pm 18^{+3}_{-8})$ MeV, which are consistent with LQCD calculations for the 1^{-+} hybrid [23]. The first uncertainties are statistical and the second are systematic. The statistical significance of the resonance hypothesis is estimated to be larger than 19σ. The product branching fraction $\mathcal{B}(J/\psi \to \gamma\eta_1(1855))\mathcal{B}(\eta_1(1855) \to \eta\eta')$ is measured to be $(2.70 \pm 0.41^{+0.16}_{-0.35}) \times 10^{-6}$. Further study with more production mechanisms and decay modes will help to identify the nature of $\eta_1(1855)$. The decay $J/\psi \to \gamma f_0(1500) \to \gamma\eta\eta'$ has also been observed $(>30\sigma)$, while $J/\psi \to \gamma f_0(1710) \to \gamma\eta\eta'$ is found to be insignificant. The ratio

$\mathcal{B}(f_0(1500) \to \eta\eta')/\mathcal{B}(f_0(1500) \to \pi\pi)$ is measured to be $(8.96^{+2.95}_{-2.87}) \times 10^{-2}$, which is consistent with the PDG value [14]. For the first time, the upper limit on the ratio of $\mathcal{B}(f_0(1710) \to \eta\eta')/\mathcal{B}(f_0(1710) \to \pi\pi)$ at 90% confidence level is determined to be 1.61×10^{-3}. The suppressed decay rate of the $f_0(1710)$ into $\eta\eta'$ lends further support to the hypothesis that the $f_0(1710)$ has a large overlap with the ground state scalar glueball [12], and the $f_0(1710)/f_0(2020)$ might be interpreted as flavor singlet [71].

[1] M. B. Cakir and G. R. Farrar, Phys. Rev. D **50**, 3268 (1994).

[2] F. E. Close, G. R. Farrar, and Z.-p. Li, Phys. Rev. D **55**, 5749 (1997).

[3] A. V. Sarantsev, I. Denisenko, U. Thoma, and E. Klempt, Phys. Lett. B **816**, 136227 (2021).

[4] A. Rodas, A. Pilloni, M. Albaladejo, C. Fernández-Ramírez, V. Mathieu, and A. P. Szczepaniak (Joint Physics Analysis Center Collaboration), Eur. Phys. J. C **82**, 80 (2022).

[5] G. S. Bali, K. Schilling, A. Hulsebos, A. C. Irving, C. Michael, and P. W. Stephenson (UKQCD Collaboration), Phys. Lett. B **309**, 378 (1993).

[6] C. J. Morningstar and M. J. Peardon, Phys. Rev. D **60**, 034509 (1999).

[7] Y. Chen et al., Phys. Rev. D **73**, 014516 (2006).

[8] L.-C. Gui, Y. Chen, G. Li, C. Liu, Y.-B. Liu, J.-P. Ma, Y.-B. Yang, and J.-B. Zhang (CLQCD Collaboration), Phys. Rev. Lett. **110**, 021601 (2013).

[9] M. Ablikim et al. (BESIII Collaboration), Phys. Rev. D **87** 87, 092009 (2013).

[10] M. Ablikim et al. (BESIII Collaboration), Phys. Rev. D **98**, 072003 (2018).

[11] C. Amsler and N. A. Tornqvist, Phys. Rep. **389**, 61 (2004).

[12] F. Brünner and A. Rebhan, Phys. Rev. D **92**, 121902 (2015).

[13] J.-M. Frère and J. Heeck, Phys. Rev. D **92**, 114035 (2015).

[14] P. A. Zyla et al. (Particle Data Group), Prog. Theor. Exp. Phys. **8**, 083C01 (2020).

[15] D. Horn and J. Mandula, Phys. Rev. D **17**, 898 (1978).

[16] N. Isgur and J. E. Paton, Phys. Rev. D **31**, 2910 (1985).

[17] M. S. Chanowitz and S. R. Sharpe, Nucl. Phys. **B222**, 211 (1983).

[18] T. Barnes, F. E. Close, and F. de Viron, Nucl. Phys. **B224**, 241 (1983).

[19] F. E. Close and P. R. Page, Nucl. Phys. **B443**, 233 (1995).

[20] P. Lacock, C. Michael, P. Boyle, and P. Rowland (UKQCD Collaboration), Phys. Lett. B **401**, 308 (1997).

[21] C. Bernard, J. E. Hetrick, T. A. DeGrand, M. Wingate, C. DeTar, C. McNeile, S. Gottlieb, U. M. Heller, K. Rummukainen, B. Sugar, and D. Toussaint (MILC Collaboration), Phys. Rev. D **56**, 7039 (1997).

[22] J. J. Dudek, Phys. Rev. D **84**, 074023 (2011).

[23] J. J. Dudek, R. G. Edwards, P. Guo, and C. E. Thomas (Hadron Spectrum Collaboration), Phys. Rev. D **88**, 094505 (2013).

[24] A. P. Szczepaniak and E. S. Swanson, Phys. Rev. D **65**, 025012 (2001).

[25] A. P. Szczepaniak and P. Krupinski, Phys. Rev. D **73**, 116002 (2006).

[26] P. Guo, A. P. Szczepaniak, G. Galatà, A. Vassallo, and E. Santopinto, Phys. Rev. D **78**, 056003 (2008).

[27] S. D. Bass, M. Skurzok, and P. Moskal, Phys. Rev. C **98**, 025209 (2018).

[28] C. A. Meyer and E. S. Swanson, Prog. Part. Nucl. Phys. **82**, 21 (2015).

[29] P. R. Page, E. S. Swanson, and A. P. Szczepaniak, Phys. Rev. D **59**, 034016 (1999).

[30] C. A. Meyer and Y. Van Haarlem, Phys. Rev. C **82**, 025208 (2010).

[31] E. Klempt and A. Zaitsev, Phys. Rep. **454**, 1 (2007).

[32] A. Rodas, A. Pilloni, M. Albaladejo, C. Fernández-Ramírez, A. Jackura, V. Mathieu, M. Mikhasenko, J. Nys, V. Pauk, B. Ketzer, and A. P. Szczepaniak (JPAC Collaboration), Phys. Rev. Lett. **122**, 042002 (2019).

[33] A. J. Woss, J. J. Dudek, R. G. Edwards, C. E. Thomas, and D. J. Wilson (Hadron Spectrum Collaboration), Phys. Rev. D **103**, 054502 (2021).

[34] H.-X. Chen, Z.-X. Cai, P.-Z. Huang, and S.-L. Zhu, Phys. Rev. D **83**, 014006 (2011).

[35] P.-Z. Huang, H.-X. Chen, and S.-L. Zhu, Phys. Rev. D **83**, 014021 (2011).

[36] W. I. Eshraim, C. S. Fischer, F. Giacosa, and D. Parganlija, Eur. Phys. J. Plus **135**, 945 (2020).

[37] M. Ablikim *et al.* (BESIII Collaboration), Chin. Phys. C **46**, 074001 (2022).

[38] M. Ablikim *et al.* (BESIII Collaboration), companion Letter, Phys. Rev. Lett. **129**, 192002 (2022).

[39] M. Ablikim *et al.* (BESIII Collaboration), Nucl. Instrum. Methods Phys. Res., Sect. A **614**, 345 (2010).

[40] M. Ablikim *et al.* (BESIII Collaboration), Chin. Phys. C **44**, 040001 (2020).

[41] X. Li *et al.*, Radiat. Detect. Technol. Methods **1**, 13 (2017).

[42] Y. Guo *et al.*, Radiat. Detect. Technol. Methods **1**, 15 (2017).

[43] P. Cao *et al.*, Nucl. Instrum. Methods Phys. Res., Sect. A **953**, 163053 (2020).

[44] S. Agostinelli *et al.* (GEANT4 Collaboration), Nucl. Instrum. Methods Phys. Res., Sect. A **506**, 250 (2003).

[45] M. Ablikim *et al.* (BESIII Collaboration), Phys. Rev. Lett. **120**, 242003 (2018).

[46] D. J. Lange, Nucl. Instrum. Methods **462**, 152 (2001).

[47] R.-G. Ping, Chin. Phys. C **32**, 599 (2008).

[48] S. Jadach, B. F. L. Ward, and Z. Was, Phys. Rev. D **63**, 113009 (2001).

[49] E. Richter-Was, Phys. Lett. B **303**, 163 (1993).

[50] W. Verkerke and D. P. Kirkby, eConf **C0303241**, MOLT007 (2003), https://inspirehep.net/literature/621398.

[51] N. Berger, B. Liu, and J. Wang, J. Phys. Conf. Ser. **219**, 042031 (2010).

[52] B. S. Zou and D. V. Bugg, Eur. Phys. J. A **16**, 537 (2003).

[53] S. U. Chung, Phys. Rev. D **48**, 1225 (1993).

[54] S. U. Chung, Phys. Rev. D **57**, 431 (1998).

[55] F. Von Hippel and C. Quigg, Phys. Rev. D **5**, 624 (1972).

[56] M. Ablikim *et al.* (BESIII Collaboration), Phys. Rev. D **93**, 112011 (2016).

[57] F. James and M. Roos, Comput. Phys. Commun. **10**, 343 (1975).

[58] C. P. Robert and G. Casella, *Monte Carlo Statistical Methods* (Springer Science, New York, 2004).

[59] J. S. Liu, *Monte Carlo Strategies in Scientific Computing* (Springer, New York, 2001).

[60] C. Langenbruch, Eur. Phys. J. C **82**, 393 (2022).

[61] D. V. Bugg, Phys. Rep. **397**, 257 (2004).

[62] M. Ablikim *et al.* (BESIII Collaboration), Phys. Rev. D **87**, 032008 (2013).

[63] M. Jacob and G. C. Wick, Ann. Phys. (N.Y.) **7**, 404 (1959).

[64] G. Costa *et al.* (BARI-BONN-CERN-GLASGOW-LIVER-POOL-MILAN-VIENNA Collaboration), Nucl. Phys. **B175**, 402 (1980).

[65] M. Ablikim *et al.* (BES Collaboration), Phys. Lett. B **642**, 441 (2006).

[66] M. Ablikim *et al.* (BESIII Collaboration), Phys. Rev. D **95**, 032002 (2017).

[67] M. Ablikim *et al.* (BESIII Collaboration), Phys. Rev. D **85**, 092012 (2012).

[68] M. Ablikim *et al.* (BESIII Collaboration), Phys. Rev. D **81**, 052005 (2010).

[69] M. Ablikim *et al.* (BESIII Collaboration), Phys. Rev. D **87**, 012002 (2013).

[70] G. D'Agostini, Nucl. Instrum. Methods Phys. Res., Sect. A **346**, 306 (1994).

[71] E. Klempt and A. V. Sarantsev, Phys. Lett. B **826**, 136906 (2022).